UNIVERSIDAD DE CHILE
FACULTAD DE MEDICINA
ESCUELA DE POSTGRADO
PROGRAMAS DE GRADOS ACADÉMICOS

ANALYSIS AND MODELING OF MICROTUBULE ARRAY SELF-ORGANIZATION

PAULA LORENA LLANOS FUENTES

THESIS TO OBTAIN THE DEGREE OF DOCTOR IN BIOMEDICAL SCIENCES

Thesis Director: Steffen Härtel.

Co-Directors: Jacques Dumais and Mauricio Cerda Villablanca.

2020

A Pablo, Pedro, Jeannette y Alejandro.

AGRADECIMIENTOS

Este camino me deja llena de aprendizajes y lecciones, pero también un profundo agradecimiento hacia las personas que fueron parte de este viaje. En primer lugar, a mi pareja, Pablo, quién me entendió, apoyó y sacó lo mejor de mí. En un sendero en ocasiones pedregoso, él hizo que cada obstáculo y momento difícil me permitiera crecer. Sin duda, gracias a su cariño, compañía y comprensión, el recorrido por esta senda fue más fácil de caminar.

Agradezco mis papás, Pedro y Jeannette; y a Alejandro, mi hermano. Ellos me han apoyado de forma absoluta en cada una de mis decisiones; han estado siempre presentes, confiando en que serán las correctas, pero también estando ahí en caso que no lo sean.

Agradezco a mi director Jacques Dumais, quién me alentó a continuar en esta carrera científica y confiar que mi formación biológica no sería un obstáculo dentro de la física, sino un aporte. Su apoyo de manera incondicional en cada uno de mis pasos produce en mí un gran agradecimiento y cariño. También agradezco a mi director Mauricio Cerda, quién siempre estuvo disponible para resolver mis dudas con una paciencia que sólo te motiva a seguir aprendiendo. Agradezco a mi director Steffen Härtel, quién me apoyó e incluyó en su laboratorio, entregándome todas las facilidades para que mi formación se completara con éxito.

Quiero agradecer especialmente a mi amigo Simón Gravelle, quién fue el Postdoc que me guio en este doctorado. En todo momento me hizo sentir capaz e inspiró a superar mis propias barreras. Me reafirmó que la libertad de pensar y el perseverar

en mis proyectos es de las experiencias más lindas que se pueden tener en ciencia, significativas enseñanzas que hoy en día me motivan a seguir por este camino.

Agradezco a mi amiga y compañera de doctorado Celia, con la que viví este proceso de cerca y con quién compartimos nuestras alegrías, frustraciones y logros. Su cariño tan sincero y su alegría contagiosa fueron pura luz en todo momento. Agradezco a todos mis amig@s querid@s, que han estado conmigo entregándome su cariño. Gracias Kanela, Milenka, Ale S., Menka, Nora, Emilie, Yiyo, Nacho B., Ale L., Dani, Ceci, Nati, Grace, Yeral, Cristobal, Vivi y Feña. Finalmente, agradezco a la secretaria del programa de Doctorado, Cecilia Carter, quién desde el primer día me apoyó, gestionando todo lo que fuese necesario para que las postulaciones, trámites y actividades resultaran bien, en ocasiones incluso sacrificando tiempo personal.

INDEX OF CONTENTS

INDEX OF FIGURES

INDEX OF TABLE

ABBREVIATIONS

+TIP Microtubule plus-end-tracking protein.

CLASP CLIP-associated protein.

CMA Cortical microtubule array.

EF1a Elongation Factor 1a.

MAPs Microtubule-associated proteins.

MT Microtubule.

MTs Microtubules.

$P_{\mathbf{zip}}$ Probability of zippering.

$P_{\mathbf{cat}}$ Probability of catastrophe.

$P_{\mathbf{x}}$ Probability of crossover.

PPB Preprophase band.

$r_{\mathbf{c}}$ Rate of catastrophe.

$r_{\mathbf{r}}$ Rate of rescue.

$r_{\mathbf{n}}$ Rate of nucleation.

$\tau_{\mathbf{eff}}$ Effective boundary pause time.

TON1 Protein TONNEAU1.

TUB1 Tubulin 1 protein.

v_g Growth velocity.

v_s Shrinking velocity.

1. RESUMEN

La orientación del plano de división celular guía la morfogénesis de tejidos en animales y plantas. Particularmente en animales, los problemas en la orientación del plano de división son la causa de enfermedades como el cáncer de colon y la microcefalia primaria autosómica recesiva; mientras que en células de plantas, las divisiones celulares orientadas incorrectamente afectan la formación y organización de los tejidos. Se han propuesto reglas homólogas de división celular para ambos tipos de células. Estas reglas consideran las propiedades geométricas de cada célula y señalan que en divisiones simétricas, el plano de división se posiciona minimizando el área y generando dos células hijas de igual volumen. Sin embargo, a diferencia de las células animales, las células de plantas, tienen una forma definida debido a la pared celular que las rodea, por lo que resulta un modelo apropiado para comprender la relación entre la forma y el posicionamiento del plano de división.

Específicamente en plantas, el mecanismo celular detrás de la localización del plano se basa en el ensamblaje de una estructura citoesquelética, la banda preprofásica o PPB, la cual está formada por microtubulos (MTs) corticales ubicados en el futuro sitio de división. En este respecto, existe una amplia evidencia de que la inestabilidad dinámica de los MTs y la interacción MT-MT contribuye a la formación de la PPB. Además, la organización de los MTs es afectada por el borde de la célula y por lo tanto por la geometría celular. Sin embargo, todavía no está claro cómo estos factores conducen a la formación y localización de la PPB.

En esta tesis, nosotros confirmamos la hipótesis que la dinámica de los MTs

y la interacción de los MTs con el borde de las célula son suficientes para explicar el posicionamiento de la PPB en configuraciones que minimlzan su área. La hipótesis fue validada usando dos líneas transgénicas del modelo biológico *Marchantia polymorpha*, Lit6b-mCitrin y tub1-GFP.

Para probar la regla de división celular, seguimos la formación del plano de división a través de microscopía confocal. En éstas imágenes medimos la proporción de células que se dividen a lo largo de los planos de división más cortos predichos por la regla de división geométrica. Este análisis mostró que el 80% de las células se dividen a lo largo del plano de división más corto, con una proporción decreciente de células que se dividen en los otros planos. Con esto, fue validada la regla de división celular geométrica en *Marchantia polymorpha*.

Luego, para estudiar la relación de la forma celular con la organización de los MTs en interfase, analizamos la orientación global de los MTs. Así, observamos que el 50% de las células dirigen los MTs siguiendo la orientación del plano más corto predicho por la regla de división celular. Por lo tanto, los MTs responden a la forma de la célula para organizar la red microtubular.

En el momento en que se finaliza la interfase (preprofase) y se gatilla la división celular, la red microtubular se auto-organiza para formar la PPB. Para estudiar este proceso realizamos un seguimiento de la PPB, para lo cual adquirimos imágenes con una alta resolución temporal y espacial de la distribución de MTs. Usando métodos cuantitativos, confirmamos que los MTs se alinean a lo largo de los planos de división predichos por la regla geométrica. Adicionalmente, encontramos que los MTs se orientan de forma ortogonal cercanos al borde de la célula. Esta característica se

incluyó en el modelo biofísico propuesto.

Posteriormente, desarrollamos el modelo biofísico con el fin de explicar la regla empírica de división. Para esto, simulamos la inestabilidad dinámica de los MTs, la interacción MT-MT y la interacción de los MTs con el borde de la célula. Al imponer un tiempo de pausa en el borde de la célula, obtuvimos una correlación entre la orientación microtubular predicha por el modelo y los patrones de MTs observados experimentalmente. De esta forma, logramos generar una estructura similar a la PPB. En resumen, en esta tesis doctoral encontramos que las propiedades dinámicas de los MTs y el tiempo de pausa en el borde celular son suficientes para explicar la formación de la PPB en una configuración que minimiza su área.

Estos resultados proporcionan la base para comprender el mecanismo dinámico detrás del establecimiento del plano de división en células de planta y podría, por analogía, contribuir a un mejor entendimiento de las enfermedades causadas por el mal posicionamiento del plano de división en células animales.

2. ABSTRACT

The orientation of cell division guides the morphogenesis of tissues in animals and plants. In animals, the mis-orientation of cell division is the cause of diseases such as colon cancer and autosomal recessive primary microcephaly. In plant cells, orientated cell divisions affect tissue formation and organization. In both animals and plants, homologous cell division rules have been proposed, which consider the geometric properties of the cell and postulate that in symmetric divisions, the division plane is positioned such that its area is minimized while producing two daughter cells of equal volume. Interestingly, plant cells have a defined shape due to the cell wall that surrounds them, so it is natural to expect a relationship between shape and the positioning of the division plane.

In plants, the cellular mechanism behind the localization of the division plane relies on the assembly of a cytoskeletal structure, the preprophase band or PPB, which is formed by cortical microtubules (MTs) at the future division site. There is extensive evidence that the dynamic instability of MTs and their mutual interactions contribute to the formation of the PPB. In addition, it has been shown that the organization of MTs is affected by the border of the cell and therefore by the cell geometry. However, it is not yet clear how these processes lead to the formation and localization of PPB.

In this thesis, we tested the hypothesis that microtubule dynamics and the interaction of MTs with the cell edges are sufficient to explain the positioning of the PPB in least-area configurations. Our hypothesis was validated using two transgenic lines of the biological model *Marchantia polymorpha*, Lit6b-mCitrin and

tub1-GFP.

To test the cell division rule in our system, we tracked the formation of new division planes. We measured the proportion of cells that divide along the shortest alternative division planes predicted by the rule. This analysis showed that 80% of the cells divide along the shortest division plane, with a decreasing proportion of cells dividing in the other planes. Hence, we validated the geometrical cell division rule in *Marchantia polymorpha*.

To study MT organization in interphase in relation to cell shape, we analyzed the global MT orientation. We found that 50% of the cells orient their MTs according to the shortest plane predicted by the cell division rule. Therefore, MTs are able to sense cell shape to organize into MT arrays.

When cell division is triggered, MTs self-organize to form the PPB. We followed this process acquiring time-lapses with a high temporal and spatial resolution of MT distribution. Using quantitative image analysis, we confirm that MTs are able to align along the alternative division planes predicted by the division rule. We also found that MTs were typically oriented orthogonal to the closest cell edge. This feature was later included in our biophysical model of MT self-organization.

A biophysical model, developed in C++, was used to simulate the dynamic instability of MTs and the MT-MT interactions within the confine of the cell geometry in order to explain the empirical cell division rule. By imposing a pause time in the cell edges, we obtained a correlation between the MT orientation predicted by the model and the experimentally observed MT patterns. Interestingly, a PPB-lie structure was formed

when the tri-dimensional cell shape was considered. In summary, in this PhD thesis we found that the dynamic properties of MTs and the pause time at the cell border are enough to explain the assembly of the PPB in least-area configuration.

These results provided a basis to understand the molecular mechanism behind the selection of a division plane in plant cells and could, by analogy, contribute to a better understanding of diseases caused by mis-positioning of the division plane in animal cells.

3. INTRODUCTION

Cell division is a defining feature of life and the basis for multicellular development in animals and plants. The fundamental processes supporting cell division are thought to be regulated by the assembly of cytoskeletal components such as actin filaments and microtubules (MTs). A common feature of cytoskeletal structures in cell division is that they are self-organized. Self-organization refers to a process whereby a stable macromolecular structure emerges from the dynamic interactions of its components (Karsenti, 2008). The most striking self-organized structures in eukaryotic cells are the mitotic spindle of animal cells and the preprophase band (PPB) of plant cells, both of which are involved in selecting the division plane of the cell (Mineyuki, 1999; Rappaport, 1985). In the case of animal cells, the division plane is dictated by the position and orientation of the mitotic spindle at late anaphase. The spindle position is set by the forces exerted by astral MTs, which extend from the centrosomes towards the cell cortex and respond to membrane cortical tension and adhesion with neighboring cells or with the extracellular matrix (Grill et al., 2001, 2003; Grill and Hyman, 2005; Paluch and Heisenberg, 2009). In contrast, the plant cells are structurally different from animal cells because they are surrounded by cell walls that dictate their shape. Thus, **the division plane in plant cells is positioned by dynamic cortical MT arrays that can "sense" cell shape to converge on configurations that minimize the area circumscribed by the PPB and, finally, produce daughter cells of nearly equal sizes** (Dixit and Cyr, 2002). There is evidence that changes in dynamic instability and the interactions between MTs drive

the dramatic rearrangement of microtubules during PPB formation (Dhonukshe and Gadella, 2003; Vos et al., 2004). However, it is still not clear how these changes could lead to the formation of a stable structure at the precise location that minimizes the area of the future division plane. **in this thesis we elucidated how cell geometry affects the self-organization of microtubules and guide the positioning of the division plane.**

3.1 Cell division orientation: Analogy between animal and plant cells.

The regulation of cell division is an essential component of development, allowing control over tissue formation. In both animal and plant cells, the mechanism controlling the orientation of the division plane involves microtubular structures. In animal cells, the orientation of cell division is determined by the alignment of the mitotic spindle while in plant cells, this process is determined by the PPB that forms prior to the assembly of the spindle (Grill et al., 2001, 2003; Grill and Hyman, 2005; Paluch and Heisenberg, 2009). The mitotic spindle and PPB are dynamic but robust MT arrays. A failure of these structures to perform their function properly can lead to defects in organ development and, in the case of animal cells, cancer (Bhowmick et al., 2004; Ingber, 2002).

MTs are polymers of α, β tubulin subunits that are remarkably conserved across eukaryotic kingdoms (Wasteneys, 2002). The same is true of microtubule-associated proteins (MAPs)(Wasteneys, 2002). The MT cytoskeleton, in animal cells, possesses a central organizer called the centrosome, from which MTs emanate and populate the cytosol. However, MTs in highly polarized cells - such as epithelial cells, skeletal

muscle fibers and neurons - are disconnected from the centrosome, forming instead a non-centrosomal array (Bartolini and Gundersen, 2006; Megraw and Kaufman, 1999) (Figure 1, left).

Plant cells offer striking examples of non-centrosomal microtubule arrays because they lack a MT-organizing center, such as the centrosome or other similar structures. Instead, plant microtubular arrays contain bundles of MTs attached to the membrane, allowing a greater diversity and dynamics of structures. The orientation of these arrays is controlled by molecular components that have clear homologs in animal cells (Wasteneys, 2002). Therefore, studying how MT arrays are organized in plant cells can give a deeper understanding of the mechanisms behind the formation of cytoskeletal structures in animal cells and beyond (Figure 1, right).

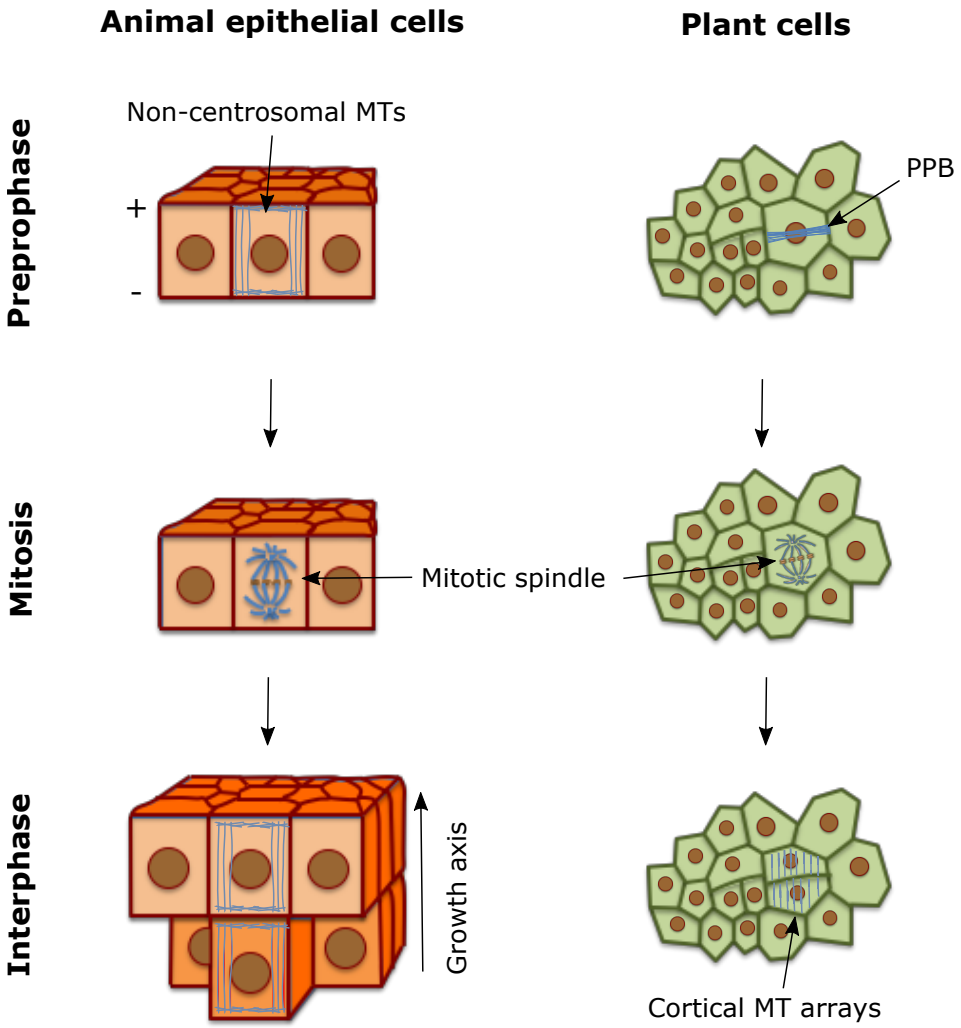

Figure 1: Non-centrosomal microtubules in epithelial and plant cells during the cell cycle.

In animal cells (left), the division plane is defined by the position of the mitotic spindle at the beginning of mitosis. In contrast, the division plane of plant cells (right) is positioned during the preprophase, when the cortical MTs form the preprophase band. The orientation of these structures regulates growth and tissue morphogenesis in animals and plants.

3.2 Establishment of the division plane in plant cells.

As mentioned above, the division plane in plant cells is determined by the location of the PPB during preprophase (Figure 2A) (Ôta, 1961; Van Damme and Geelen, 2008).

The PPB persists throughout prophase but is disassembled upon nuclear envelope breakdown as the mitotic spindle forms (Figure 2B) (Dixit and Cyr, 2002). After the disappearance of the PPB, cortical actin microfilaments are sparse in the future division site, forming an actin-depleted zone (Cleary et al., 1992; Liu and Palevitz, 1992). The actin-depleted zone maintains the division site prior to cytokinesis, in addition to the correct mitotic spindle orientation (Figure 2B-D) (Kojo et al., 2013). Typically, the mitotic spindle is oriented perpendicular to the plane delineated by the PPB, thus leading to the proper segregation of chromatids between the two daughter cells. Cytokinesis follows chromatids segregation with the formation on the cell plate by the phragmoplast (Figure 2C-D), a cytoskeletal structure whose MTs are perpendicular to the division plane and act as scaffolding to build the new cell wall (Jürgens, 2005). In particular, the MTs of the phragmoplast direct the traffic of secretory vesicles to the center of the dividing cell. Accumulated vesicles undergo fusion and fission thus depositing polysaccharides and structural proteins to form the cell plate. The nascent cell wall is inserted into the parental wall at the cortical division site previously occupied by the PPB (Figure 2D) (Drakakaki, 2015). **The faithful coincidence between the position of the cell plate and the PPB makes the PPB the ideal marker for the selection of the division plane** (Müller et al., 2009; Rasmussen et al., 2013; Smith, 2001; Van Damme and Geelen, 2008). However, how the PPB itself is positioned at the division site remains a mystery more than 50 years after its discovery (Pickett-Heaps and Northcote, 1966).

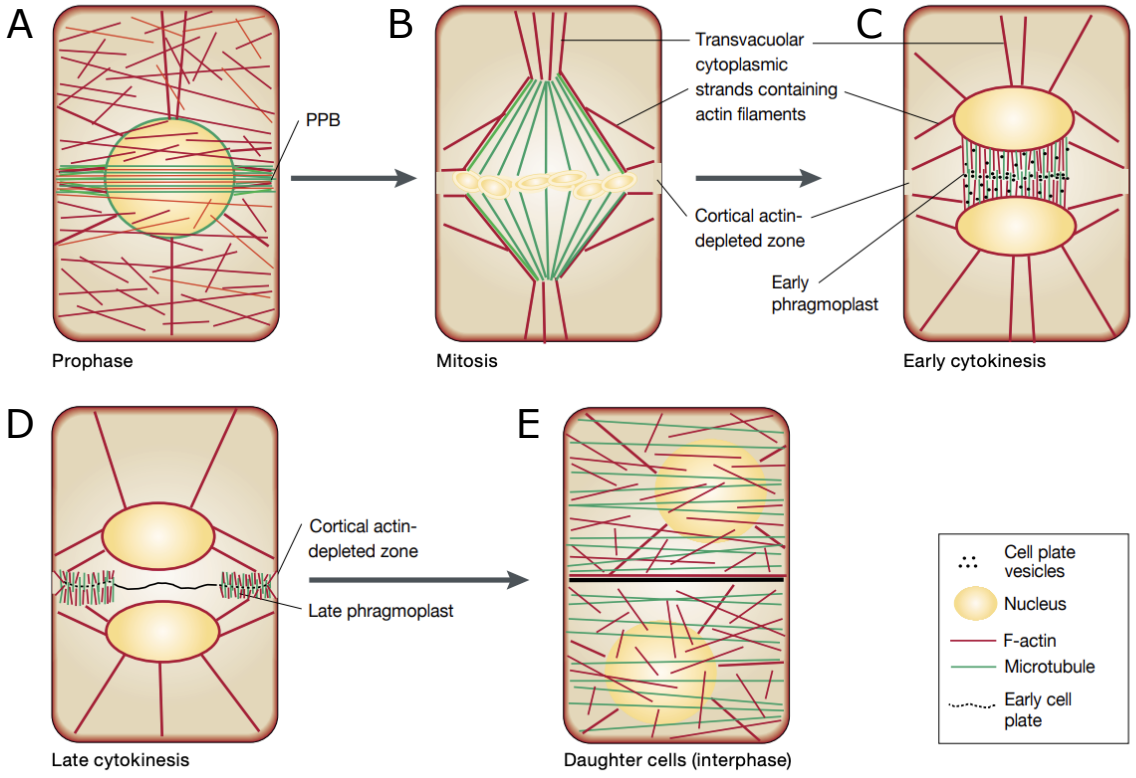

Figure 2: Cytoskeleton organization during symmetrical cell division.

A, During prophase, the PPB circumscribes the future division plane. **B**, The PPB is disassembled upon entry in mitosis, leaving behind an actin-depleted zone in the cell cortex, which persist and marks the division site throughout mitosis and cytokinesis. **C-D**, After completion of mitosis, the phragmoplast grows between the daughter nuclei until it reaches the parental plasma membrane and cell wall, previously marked by the PPB. **E**, When the mitosis is finished, the MTs are located around the cell membrane to form the cortical MT array of interphase. Figure from Smith et al., 2001.

3.3 Factors involved in the positioning and formation of the preprophase band.

3.3.1 Cell shape.

The superficial aspects of cell division have been studied extensively during the second half of the nineteenth century which has led to a variety of geometrical

division rules. Julius Sachs proposed that plant cells tend to divide into two equal cells with a division plane at right angle to the pre-existing walls (Sachs, 1878). A few years later, Leo Errera proposed an interesting refinement to Sachs' rule (Errera, 1886). He drew a parallel between plant cells and soap bubbles and posited that a cell minimizes the surface area of the new division plane (Figure 3). Errera and Sachs division rules can be paraphrased in modern terms as: **the PPB, and subsequently the cell plate, adopts configurations of minimal surface area that enclose a fixed cellular volume.**

Despite its predictive power, Errera's Rule has been the subject of criticisms, mainly because exceptions to the rule have been noted repeatedly (Serna and Fenoll, 2003). **In this respect, the Dumais group has shown that the majority of exceptions to this rule represent alternative division planes that fulfill Errera's rule locally, rather than globally** (Besson and Dumais, 2011). They demonstrated that the selection of the division plane involves a competition between alternative configurations whose geometries represent local area minima. The probability of observing a particular division configuration increases inversely with its relative area according to an exponential probability distribution known as the Gibbs measure. This modern rule for cell division has been re-evaluated in other types of plant cells, confirming the rule in most cases, although interesting improvement have also been suggested (Louveaux et al., 2016; Purswani, 2014; Shapiro et al., 2015; Yoshida et al., 2014). In addition, Besson and Dumais proposed that the empirical division rule is made possible by tense cytoskeletal elements that force the PPB into configuration of least area. Recently, Louveaux and coworkers have demonstrated a close parallel

between the direction of maximal tension in the cell, microtubule orientation and division plane selection; confirming that MTs are central to the selection of the division plane in accordance with the cell's geometry (Louveaux et al., 2016).

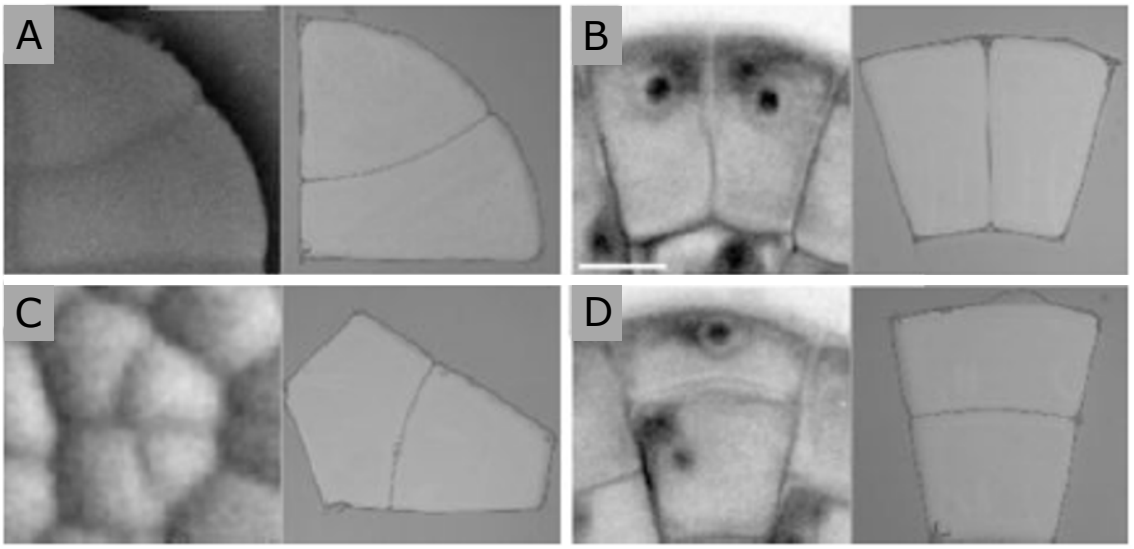

Figure 3: Errera's Rule predicts how plant cells divide.
Each pair of images shows a dividing cell (left) and the configuration of two soap bubbles confined to the same geometry (right). **A**, Quadrant cell of a glandular trichome of *Dionaea*. **C**, Meristematic cells of *Zinnia elegans*. **B** and **D**, Marginal cells of the green alga *Coleochaete*. Figure from Besson & Dumais, 2011.

3.3.2 Nucleus position.

During cell division, another important event linked to PPB formation is the migration of the nucleus to the center of the cell, a process controlled by actin microfilaments and MTs growing out from the nuclear surface to the cell membrane (Grolig, 1998). Initially, the MTs grow out in all direction but become gradually restricted while the nucleus becomes located in the centroid of the cell and the PPB is formed around it. Nuclear positioning seems to play an important role during division site establishment

in symmetric division (Galatis et al., 1984; Katsuta et al., 1990; Kennard and Cleary, 1997; Lloyd and Traas, 1988; Mineyuki and Palevitz, 1990; Murata and Wada, 1991; Venverloo and Libbenga, 1987). However, nuclear positioning alone cannot explain how the PPB is located because for a given cell geometry, many PPB positions are possible around the cell's centroid and yet only some of these positions are in fact observed experimentally. Therefore, both nuclear positioning and cell geometry are relevant factors in division plane selection.

3.3.3 Interphase microtubule array.

The selection of the division plane has been related to the principal direction of growth, geometrical rules, and nucleus position. However, it is still unclear how the orientation of the cortical microtubule array, CMA (Figure 2E), that coordinates the growth direction and cell elongation, could influence the division plane positioning.

The higher plant cells do not possess a centrosome as animal cells. Instead, the microtubules organizing activity is located around the cell cortex without a specific pattern and it has been proposed that specific array are achieved by a self-organized mechanism (Schmit, 2002). Self-organization is associated with systems consisting of a large number of nearly identical elements (e.g. MTs) undergoing numerous local interactions among each other, in a non-equilibrium environment (Karsenti, 2008).

The CMA in a rapidly elongating cell is typically arranged transverse to the elongation axis of the cell (Granger and Cyr, 2001; Sugimoto et al., 2000). By extension, it has been suggested that the orientation of the CMA is kept during preprophase although

this proposal remains untested. During interphase, in cells that are not dividing, the CMA is a dynamic structure that does not maintain a fixed orientation in time. For example, in hypocotyl epidermal cells, which share a characteristic elongated shape, it is possible to find different MT patterns (Ehrhardt and Shaw, 2006; Thoms et al., 2018). Studies about the changes of MT arrangement could allow us to understand the dynamic features of MTs in interphase.

Vineyard et al, 2013 observed that the creation of a coaligned MT array requires coordination across multiple faces. Moreover, during this transition, the array organization is driven primarily by the creation and retention of transverse MTs and the depolymerization of longitudinal MTs. However, the organization process includes temporal disorganization before a coordinated transverse MT arrangement is achieved between anticlinal and periclinal faces (Vineyard et al., 2013). A recent study has simulated the CMA in embryos of *Arabidopsis thaliana* (Chakrabortty et al., 2018) considering cell shape, edge restriction, and parameters of MT dynamics to simulate the distribution of MTs. The authors could reproduce the distribution of CMA and predict the division planes observed experimentally. However, the model could reproduce the cell division planes only until 16 cell-stage.

Thus, experimental and theoretical evidence shows that CMA in interphase can influence PPB orientation and, consequently, the localization of the division plane; although more studies are necessary to demonstrate how MT self-organization explains these observations.

3.3.4 Molecular factors.

Many molecular factors are part of the PPB beyond microtubules. The TTP complex (TON1-TRM-PP2A) is a protein assembly involved in the spatial organization of cortical microtubules, including the PPB (Schaefer et al., 2017; Spinner et al., 2013). It is important to consider the relevance of this complex given that plant cells lack the centrosomes found in animal cells. In particular, TON1 has an important role in the narrowing of MT arrays during PPB formation, which is coordinated with cell-cycle progression by mitogenic signals (Costa, 2017). Other proteins from the TTP complex are the TRM proteins, which include TRM6-8. The Arabidopsis trm678 mutant causes almost total disruption of the PPB in root cells. Although the mutant does not induce widely aberrant cell division patterns, it causes a loss of precision in cell division orientation and as major effects on spindle positioning (Schaefer et al., 2017).

The molecular components described previously allow us to understand how MTs can form a narrow band from a cortical MT array, however, more studies are needed to understand the location of the PPB considering the geometrical aspects followed to establish the division plane. A +TIP protein, CLASP, has been put forward as a modulator between MTs and the cell edges. During the preprophase, CLASP accumulates only on the edges intersected by the band, where it stabilizes the MTs that reach the sharp edges, promoting the formation of bundles of MTs (Ambrose et al., 2011). Moreover, transgenic line co-expressing GFP-CLASP1 and RFP-Tubulin6 showed colocalization of both signal in transfacial microtubules on sharp edges (Ambrose et al., 2011). The sharp edges could be a local physical barrier

because MTs require extra energy to bend the tubulin lattice to pass from one face to another. Therefore CLASP would act by buffering that effect allowing the stabilization of MTs in that zone. Accordingly, in the clasp-1 mutant, sharp edges induce depolymerization and catastrophe of MTs, with a consequent decrease in transfacial MTs (Ambrose et al., 2011). In vitro studies showed a concentration-dependent ability to increase rescue frequency, decrease catastrophe frequency, and slow the microtubule depolymerization rate (Al-Bassam et al., 2010; Bratman and Chang, 2007). Other studies have indicated that CLASP, in the presence of other factors, acts as a pause inducer of MTs (Moriwaki and Goshima, 2016). Additionally, CLASP regulates EB1 localization, which accumulates at growing MT plus-ends, influencing the MT dynamics and polarization (Akhmanova and Steinmetz, 2008, 2010; Coquelle et al., 2009; Galjart, 2010; Guesdon et al., 2016; Morrison, 2007).

3.3.5 Dynamics of microtubules in the preprophase band.

The microtubules and microfilaments of actin, together with MT associated proteins (MAPs), are able to self-organize into stable structures such as the PPB (Palevitz and Hepler, 1974; Pickett-Heaps, 1974; Subramanian and Kapoor, 2012). The PPB is thought to be formed by a rearrangement of pre-existing MTs in the cell membrane (cortical MTs), newly initiated MTs on the nuclear surface are transported to the PPB cortical site (astral MTs) and MTs initiated directly at the PPB cortical site (Panteris et al., 1995). MT growth is initiated by nucleation in spatially disperse sites catalyzed by a complex of γ-tubulin protein (Teixidó-Travesa et al., 2012). After nucleation, periods of shrinkage (catastrophes) and growth (rescue) follow each other

in a GTP-dependent process called **dynamic instability** (Figure 4A) (Gardner et al., 2013). Dynamic instability is most pronounced at the plus-end of microtubules; while the minus-end presents mainly static or shrinking states (Ehrhardt and Shaw, 2006). As a consequence of these two states, the growing plus-ends can collide with other MTs. Experiments have shown that these collisions can have three possible outcomes whose relative probability of occurrence is determined by the angle of collision. The first outcome known as **zippering** occurs when the incoming MT changes its direction and grows alongside the MT it encountered. The second outcome, termed **induced catastrophe**, is when the incoming MT switches to the shrinking state. Finally, the incoming MT can **cross over**, that is, it keeps growing in its original direction (Figure 4b) (Dixit and Cyr, 2004). Strikingly, during PPB formation, the probability of transition between growing and shrinking phases in cortical microtubules outside the PPB increases significantly, which has been proposed has a mechanism to achieve an ordered structure such as the PPB (Dhonukshe and Gadella, 2003; Vos et al., 2004). Both dynamic instability and collisions between MTs can produce order, although it is still unclear which of the collision outcomes is necessary and/or sufficient to explain the ordering process seen during PPB formation. To gain a better understanding of the complexity of cell division, many biologists have turned to biophysical modeling in order to capture the dynamics of MT structures (Allard et al., 2010; Ambrose et al., 2011; Ambrose and Wasteneys, 2012; Eren et al., 2010, 2012; Tindemans et al., 2010).

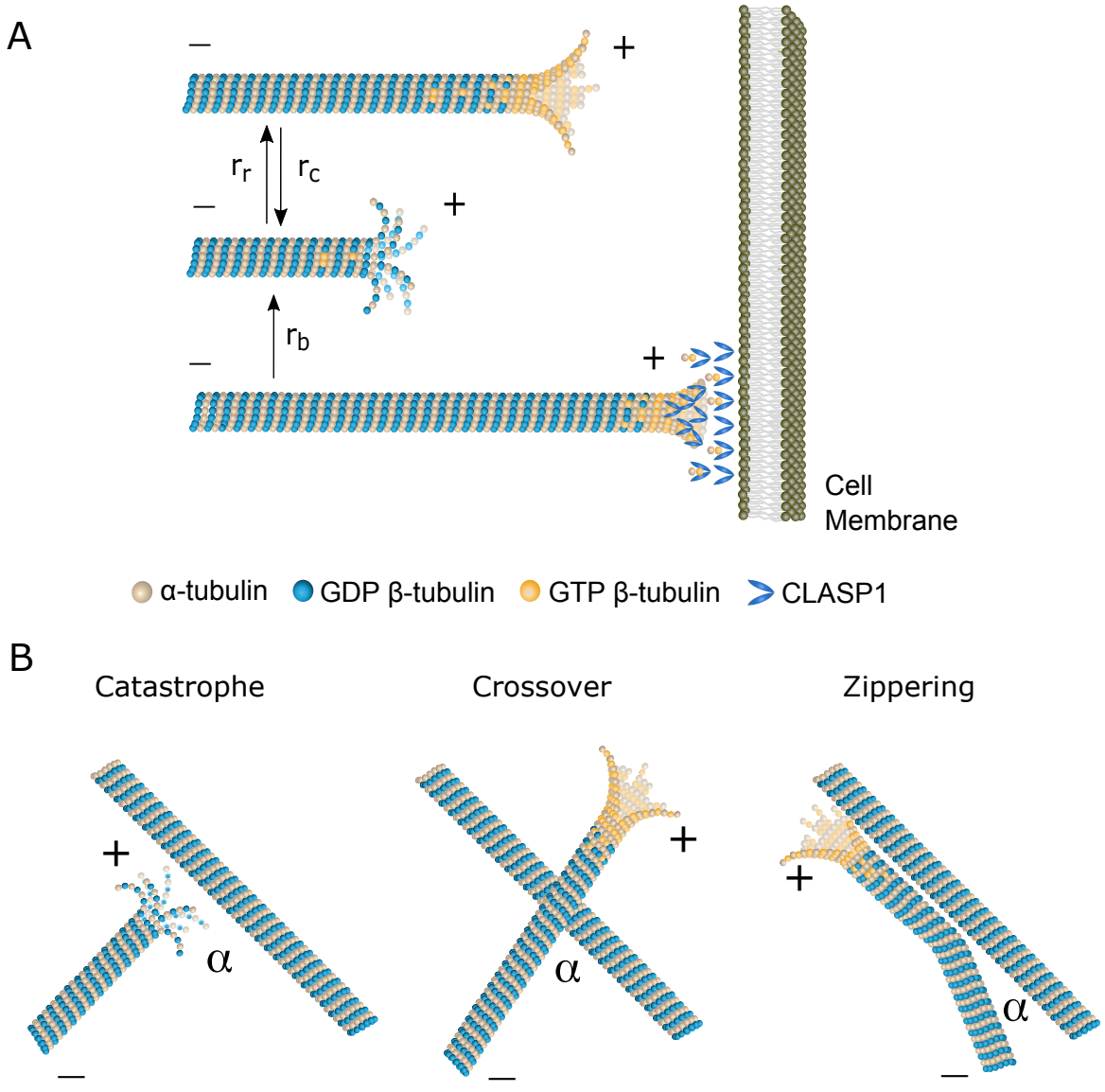

Figure 4: Schematic overview of the dynamic properties of microtubules.

Scheme of the dynamic properties of MTs and their molecular components. Microtubules are polymers of α/β tubulins with plus (+) and minus (-) ends that present a high and low rates of polymerization, respectively. **A**, From top to bottom is shown the states of the dynamic instability of MTs: growing, catastrophe and pause. The transition rates have been quantified based on microscopic observations, which are represented by r_g for growing rate, r_c for catastrophe rate and r_b for pause rate. **B**, The MT-MT collision outcomes are approximated by probability functions that depends on the α angle between MTs.

3.4 Modeling microtubule dynamics.

MT dynamics is influenced by a wide range of factors such as molecular signaling, MT binding protein, internal and external constraints, local cell curvature, etc. **Quantitative models are a way to integrate this complex network of interactions and arrive at a clear understanding of MT self-organization during cell division**. A successful strategy to elucidate the behavior of MTs is stochastic modeling, which can incorporate explicitly the randomness of molecular processes. In particular, the parameters for MT zippering, induced catastrophe and cross-over can be modeled as random variables with a probability distribution that depends on the angle of collision between MTs (Figure 4B). Those parameters have been used to model the alignment and organization of cortical MTs, taking into account the intrinsic dynamics and interactions between microtubules (Allard et al., 2010; Eren et al., 2010; Hawkins et al., 2010; Tindemans et al., 2010). However, few of the models published previously can explain how cell shape can help organize the cortical microtubule arrays in specific orientations. In a few cases, some improvements have been considered by adding special conditions for MTs reaching the cell border (Ambrose et al., 2011). For example, if we include a catastrophe state as a boundary condition, the MTs tend to align with the closest cell border. In contrast, when a pause state is included as a boundary condition, the MTs align at right angle with the cell's border (Ambrose et al., 2011). Therefore, it is clear that the boundary conditions are an important element of any model that aims to study the alignment of MTs in a realistic cell. To improve the modeling of MT self-organization, a number

of recent publications have ascribed an important role to the MT-severing enzyme katanin, both in setting up the alignment of the cortical array, as well as in guiding its reorientation in response to external cues (Bichet et al., 2001; Bouquin et al., 2003; Burk et al., 2001; Stoppin-Mellet et al., 2002). Based on these observations, Deinum and coworkers provided a mechanistic understanding of why severing is fundamental for inducing rapid changes in MT organization (Deinum et al., 2017).

In parallel, the dimensionality of modeling (2D versus 3D models) has been discussed as an important factor in understanding the formation of MT networks. To date, most of the simulations have been developed on 2D surfaces. Recently, the influence of 3D growth on MT organization was studied in elliptical cells and embryos cells of *Arabidopsis thaliana* (Chakrabortty et al., 2018; Mirabet et al., 2018). They found that because of directional persistence, microtubule growth invariable leads to cortical arrays, even when the MTs have the freedom to release from the membrane. Chackrabortty et al. could reproduce the CMA on the realistic shape of embryo cells and predict the division plane until the 16-cell stage of embryo development. However, more robust 3D models are still needed to explain MT self-organization and their ability to select a division plane in plant cells.

Although the dynamic properties of MTs are considered sufficient to get ordered cortical arrays, it is still unknown whether these properties are sufficient to explain how microtubules sense cell shape and adopt least-area configurations when forming the PPB.

4. HYPOTHESIS AND OBJECTIVES

We are testing the hypothesis that **microtubule dynamics and the interaction of microtubules with the cell edges are sufficient to explain the positioning of the PPB in least-area configurations**. Microtubule dynamics are encapsulated by the parameters that describe the dynamic instability, interaction with the edge, and MT-MT interactions, such as zippering, cross-over and induced catastrophe (Figure 4). This hypothesis will be tested by incorporating the probability functions of MT dynamics in a biophysical model and confirming whether these parameters are sufficient to explain the positioning of the division plane.

General objective: Evaluate through *in vivo* observations and biophysical modeling the importance of dynamic instability of microtubules, MT-MT interaction and the interaction of the microtubules with cell edges on the formation and positioning of the PPB in least-area configurations.

Specific objective 1: Quantify the spatial distribution of microtubules in cells undergoing division.

Specific objective 2: Develop a biophysical model of microtubule dynamics and cell border interactions during the preprophase band formation.

Specific objective 3: Test the biophysical model using mutants to perturb the dynamics of microtubules.

5. METHODOLOGY

This section contains methods for the plant culture, confocal imaging, and image analysis tools. We developed algorithms for image analysis that were described to guide future users.

5.1 Plant materials and growth conditions.

The liverwort *Marchantia polymorpha* was used as a model system to analyze the cytoskeletal dynamic during cell division. *Marchantia* is a bryophyte with a rapid life cycle. It is easy to propagate and because of its small size haploid genome (approximately 280 Mb), several transgenic lines have been developed during the last years. *Marchantia* has vegetative structures called gemmae, with a simple easy-to-image architecture. Also, the gemmae are well suited for quantitative cellular imaging due to their prostrate morphology and exposed mode of development. Gemmae have cells actively dividing in the notch area that allow us to acquire numerous highly resolved time-lapse sequences of dividing cells (Figure 5). Moreover, *Marchantia* was recently shown to follow the stochastic division rule (Purswani, 2014).

Marchantia was grown in soil (50% perlite and 50% peat moss) under long-day conditions (16h light/8h dark) at 21℃ and 70% humidity. GFP-MpTUB1 and Lit6b-mCitrin transgenic lines were used, both transgenes under the control of the Elongation Factor 1a (EF1a) promoter. GFP-MpTUB1 was provided by Prof. Henrik Buschmann from Osnabruk University, Germany (Buschmann et al., 2016) and Lit6b-mCitrin line was provided by Prof. Jim Haseloff (Cambridge University)

(Figure 6B-C).

The *Marchantia* transgenic line, GFP-tubulin1, was developed and characterized to get a model system that allows us to study MT dynamics during cell division. The β tubulin 1 construct was shown to be functional because the protein was incorporated into microtubules in cultured tobacco BY-2 cells and *Marchantia* cells. Consequently, **the *Marchantia* line obtained did not show morphological alterations in cell division structures, including the PPB. On the other hand, our results showed shrinking and growing velocities accordant with the velocities published for *Arabidopsis thaliana*. Therefore, the dynamic instability of MTs is not perturbed in this transgenic line.**

Arabidopsis thaliana was grown in soil (100% peat moss) under long-day conditions (16h light/8h dark) at 21° and 70% humidity. We used the wild-type and trm678 mutant lines that express mCitrine-KA1 under the control of pPDF promoter. KA1 is a domain that interact with the membrane by anionic phospholipids. The wild-type line was provided by Prof. Olivier Hamant from ENS-Lyon, France, and mutant line was provided by Prof. David Bouchez from INRA-Versailles, France (Schaefer et al., 2017).

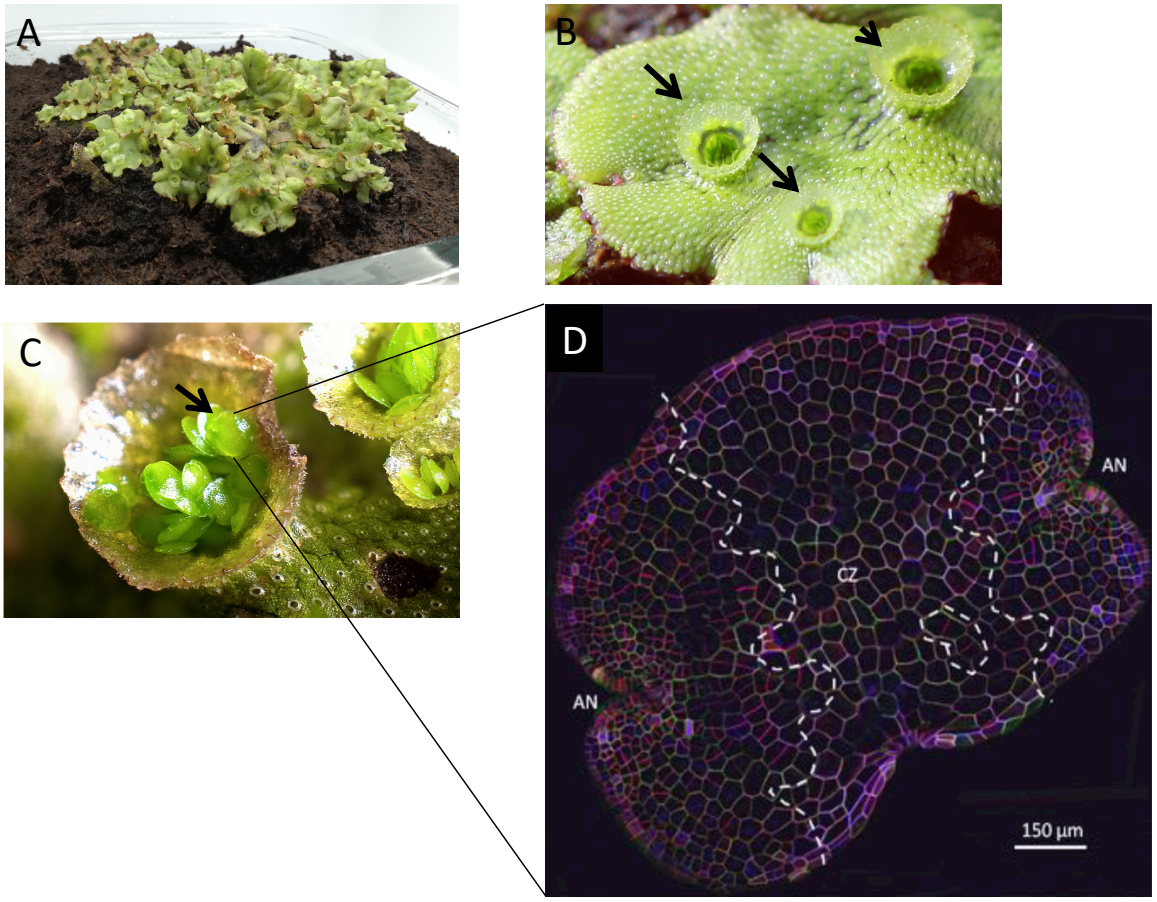

Figure 5: Our biological model: *Marchantia polymorpha*.

A, Culture of *Marchantia* in the laboratory. **B**, Vegetative splash cups on the thallus of *Marchantia*, an asexual reproductive structure (black arrows). **C**, Splash cups containing lens-shaped propagules called gemmae (black arrows). All of the photos were taken from *Marchantia* culture in the laboratory . **D**, Confocal image of a gemma expressing the EF::GFPLTI plasma membrane marker. The white dashed lines separate the two regions of dividing cells known as apical notches (AN) from the central zone (CZ) of non-dividing cells. Confocal image from the Ph.D. thesis of Nuri Purswani, 2014.

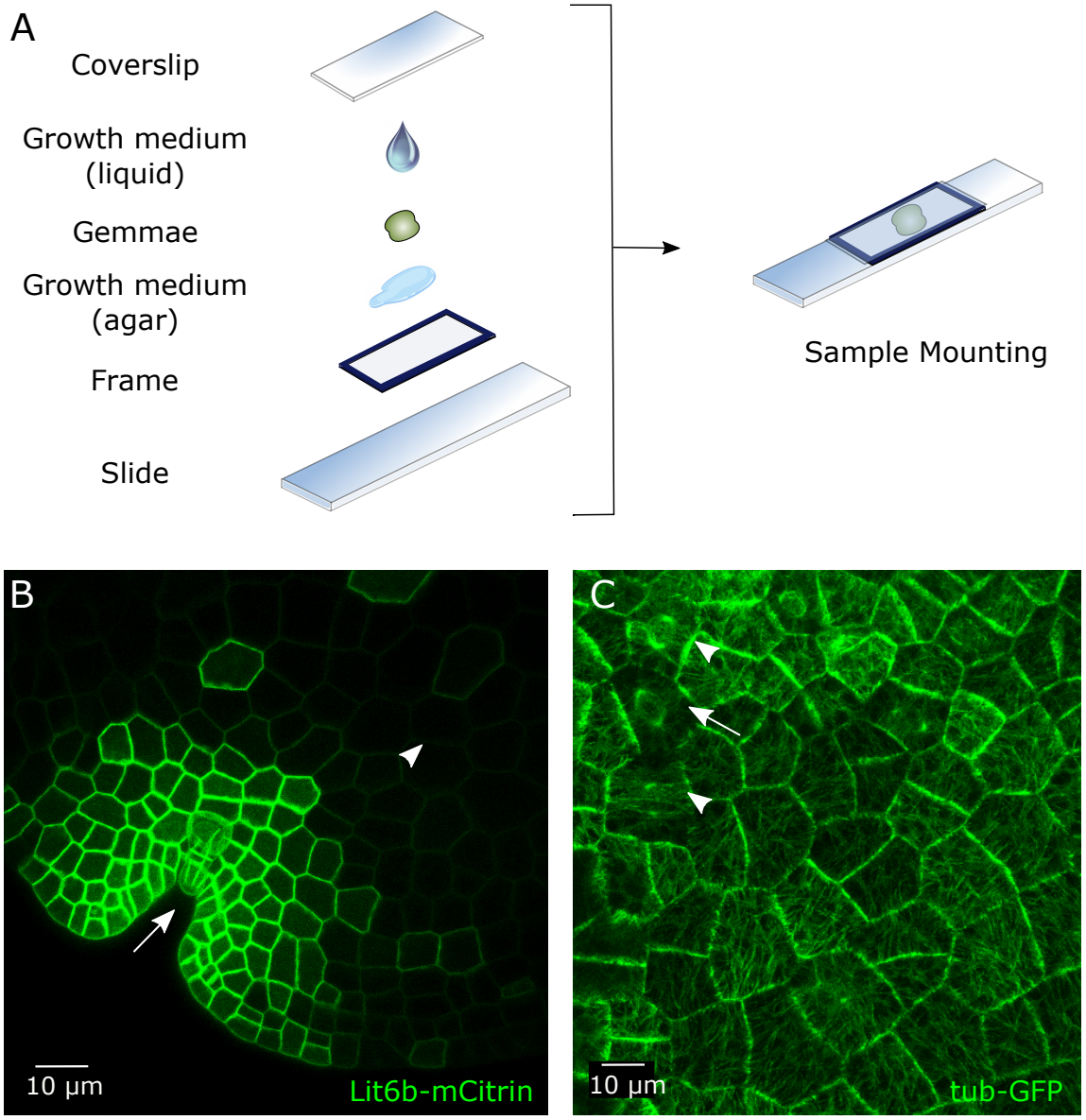

Figure 6: The mounting of *Marchantia polymorpha* for fluorescence imaging.

A, Setup used to observe the gemmae. **B**, Membrane signal in notch of the gemma from the Lit6b-mCitrin line (green). The arrow shows the meristematic zone of the notch. The arrowhead shows the zone with low rate of cell proliferation. **C**, Microtubules signal in notch of the gemma from the GFP-TUB1 line (green). Arrowheads show PPB formation and the arrow shows the polar organizers formed prior to the PPB. textbfB and textbfC are images from confocal microscopy

5.2 Image acquisition.

Gemmae were removed from splash cups and transferred to 1.58 g/L Gambor B5 agarose media plates (Duchefa Biochemie G0210). The cell division was induced in gemmae by incubation during two days in a growth chamber at 22℃ under long day cycle of 16h light and 8h dark. Long-term live cell imaging observation of the sample was performed using a chamber to use under microscope. The growth chamber is represented in the Figure 6A. We glued a frame on the coverslip (Geneframe AB0577, Thermofisher), and we add Gambor B5 agar media. Gemmae was placed on the Gambor B5 agar medium and covered with a drop of Gambor B5 liquid medium to finally cover with the coverglass. The samples were observed immediately after the growth chamber preparation.

Arabidopsis meristems were cut from the stem, dissected an hour before imaging, and stuck in "*Arabidopsis* apex culture medium" (2.2 g/L Duchefa Biochemie MS basal salt mixture without vitamins, 1% sucrose, 0.8% agarose, pH 5.8). The medium was supplemented with vitamins (0.1 g/L myo-inositol; Sigma), nicotinic acid (1 mg/L; Sigma), pyridoxine hydrochloride (1 mg/L; Sigma), thiamine hydrochloride (10 mg/L; Sigma), glycine (2 mg/L; Sigma).

5.3 Microscopy platform.

Time-lapse microscopy was performed using a Leica SP8 upright microscope (Leica Microsystems, Germany) equipped with a $40X$, 1.3 N.A, oil immersion objective. Images were acquired at a period among 15 to 40 minutes depending of PPB

progression. Microscope images size was $1024x1024$ pixels with a resolution of $0.0789\,\mu$m/pixel. The images were named by date of the observation, the field of view and the time-step, starting with time 0 minutes. Therefore, the name was registered as "YYYYMMDD fieldN tN". An excitation wavelength of $488\,$nm was utilized to detect GFP-tubulin and Lit6b-mCitrine with emission lengths collected between $510-535\,$nm. The z-stacks collected by field was defined with fine step sizes of 0.5 to $0.7\,$nm.

The observation of the MT growth dynamic was performed with a spinning disk confocal inverted Zeiss microscope (AxioObserver Z1, Carl Zeiss Group, Germany) equipped with a spinning disk module (CSU-W1-T3, Yokogawa, Japan) and a ProEM+ 1024B camera (Princeton Instruments, USA) using a $100\,$x PlanApochromat objective (numerical aperture 1.46, oil immersion). GFP was excited with a $488\,$nm laser ($150\,$mW) and fluorescence emission was filtered by a $525/50\,$nm BrightLine® singleband bandpass filter (Semrock, USA). Images were acquired with $200\,$ms exposure time by frame and $10-15\,$s of period.

The imaging of shoot apical meristem (SAM) of *Arabidopsis* was performed with a confocal microscope Leica SP8 upright scanning equipped with a water immersion objective (HCX IRAPO L $25\,$x/$0.95\,$W). Fluorophores were excited using led laser (Leica Microsystems, Wetzlar, Germany) emitting at wavelengths of $514\,$nm for mCitrine and the signal was collected at 521–$550\,$nm for mCitrine, The following scanning settings were used: pinhole size $1\,$AE, $1.25\,$x zoom, scanning speed of $8000\,$Hz (resonant scanner), frame averaging 4, Z intervals of $0.5\,\mu$m.

5.4 Image processing.

The raw z-stack of each field acquired was analyzed to select and crop the area that contain the cell in the cell division process (Figure 7A-B). This z-stack cropped was filtered using a CSSBDeep plugin of Fiji (Figure 7C), which is a a deep-learning toolbox for microscopy image restoration with a command for deconvolution of microtubules (Weigert et al., 2018). A subset of slices of the original z-stacks were selected, which contained the cortical MT signal of the cell (Figure 7D). This subset of z-stack and a z-projection image was saved in the correspondent folder (Figure 7E).

To get the cell geometry, a second z-projection was obtained with deeper slices selection from the original z-stack, and without the upper slices to avoid the microtubule cortical signal. The cell contour was drawn using the MATLAB algorithm developed and published by Besson and Dumais, 2011. Specifically, this algorithm was used to get the cell contour, vertices and the alternative division planes.

We developed a MATLAB routine where the contour was drag to a position that fit with the cortical microtubule signal of the z-projected image of the same cell (Figure 7E). Additionally, in the developed MATLAB routine, we removed the microtubule signal outside of the cell border, this image was saved in a correspondent folder (Figure 7F).

The vector field, representing the local MT orientation, was obtained by OrientationJ, a Fiji plugin (Figure 7G). The data was exported as a '.csv' using a macro code allowing us to analyze a batch of images.

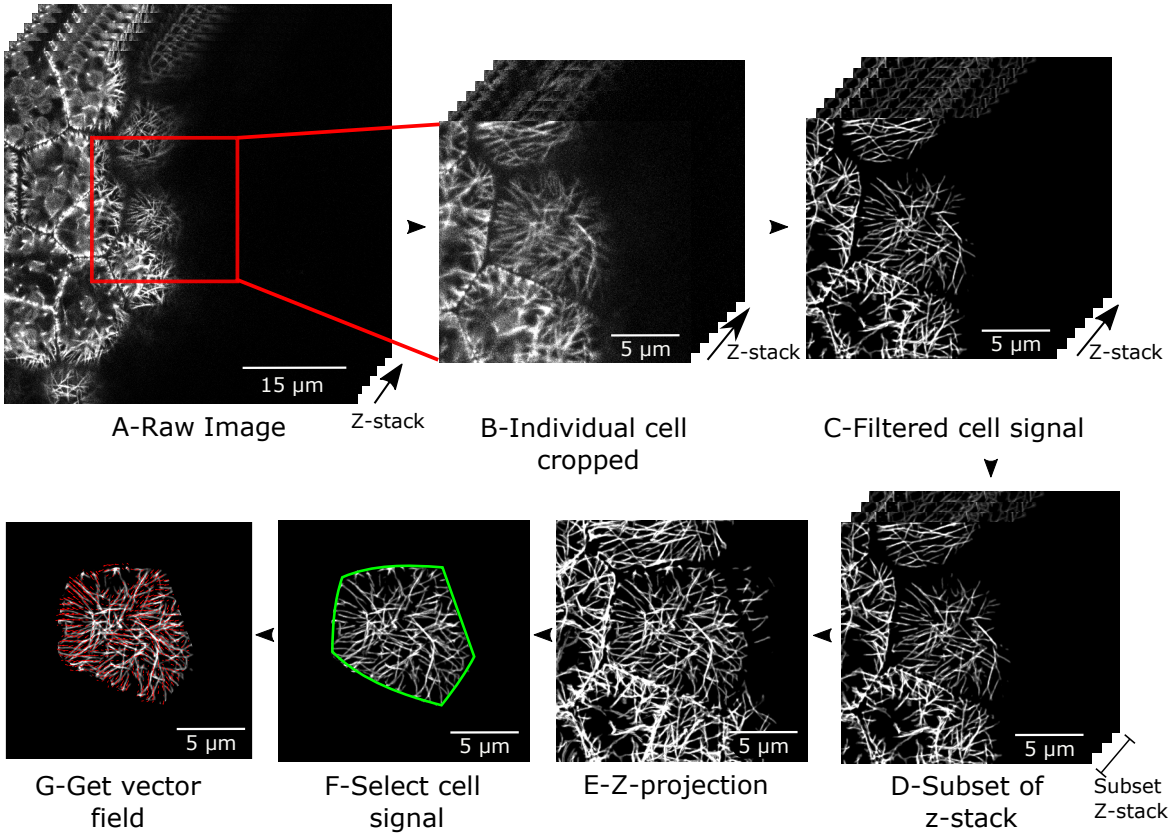

Figure 7: General scheme for image processing.

A-B, The raw z-stack of images with MT signal was cropped to get individual cells of interest (red square in A and panel B). **C**,The cropped z-stack of cell images was filtered using the CSBDeep Fiji plugin. **D**, A subset of the z-stack was selected to get the slices with the cortical microtubule signal and the slices with the cell contour signal (middle slices). **E**, The selected z-stack subsets were projected to get the MT signal and cell shape. **F**, Using a MATLAB routine, the cell shape was drawn and it was used to remove the signal outside of the cell area. **G**, The resulting masked image was used in OrientationJ, a Fiji plugin to get the vector field of MT orientation. The vector field was exported for other quantitative analyses.

5.5 Image analysis

5.5.1 Test of the geometrical rule.

The geometrical rule was tested in *Marchantia* cells using three datasets of images:

the cells before and after cell division expressing Lit6b-mCitrin, the cells expressing

tub1-GFP in interphase and during the PPB formation (time-lapse images). The image processing has been described in section 5.4. To draw the cell contour and predict the alternatives division plane we used the MATLAB routine published by Besson and Dumais, 2011. Each of the four alternative division planes predicted (modes) corresponds to a possible solution of Besson-Dumais, (1) cuts the cell in two equal parts, (2) represents the local minimal length and (3) intersects the edge with a right angle right angle with edge. The mode 1 is the shortest and the mode 4 is the longest division plane predicted. Thus, we extracted the coordinates and length from each alternative division and the area of the cell.

To test the cell division rule in the dataset of the cells expressing Lit6b-mCitrin, we used a z-projection image of the upper slices of z-stack after the cell division to can define the cell contour. The experimental division planes observed were compared with each alternative division plane predicted in order to classify them either as "mode 1", "mode 2", "mode 3", "mode 4" or other. The frequency of each mode in the dataset was represented in a histogram plot.

The probability (p_{ij}) to observe a particular division plane among two competing planes i and j, where the length of i (l_i) is smaller than the length of j (l_j), is given by the Gibbs measure, which can be written as:

$$p_{ij} = \frac{n_i}{n_i + n_j} = (1 + e^{-\beta\delta_{ij}}), \tag{1}$$

where δ_{ij} is the relative length difference $(l_j - l_i)/\sigma$, σ is the mean cell diameter defined as the square root of the cell area. n_i and n_j are the numbers of cells

dividing through plane i and j, respectively, and β is the parameter determined by interpolating the data to an exponential curve. The Gibbs measure was obtained using a MATLAB routine developed.

5.5.2 Microtubule distribution based on geometrical rule.

The cell contour, the alternatives division planes and the vector field were obtained following the steps described in the section 5.4. We defined a band of finite width ($2\mu m$) that surround each of the four modes, and only the vectors within the band were used for the projection (magenta curves, Figure 8).

We calculated the inner angle (θ) among the local MT orientation ($\vec{v}$) and the closest tangent to the division plane ($\vec{t}$) (Figure 8, Eq. 2). To evaluate the alignment ($Projection$) of the vectors with the division plane we calculated the sum of the projection of the inner angle (θ) (Eq. 3), where N is the total vectors evaluated.

$$\theta_i = acos\left(\frac{\vec{t_i} \cdot \vec{v_i}}{\|\vec{t_i}\|\|\vec{v_i}\|}\right), \tag{2}$$

$$Projection = \frac{\sum_{i=1}^{N} cos(2\theta_i)}{N}. \tag{3}$$

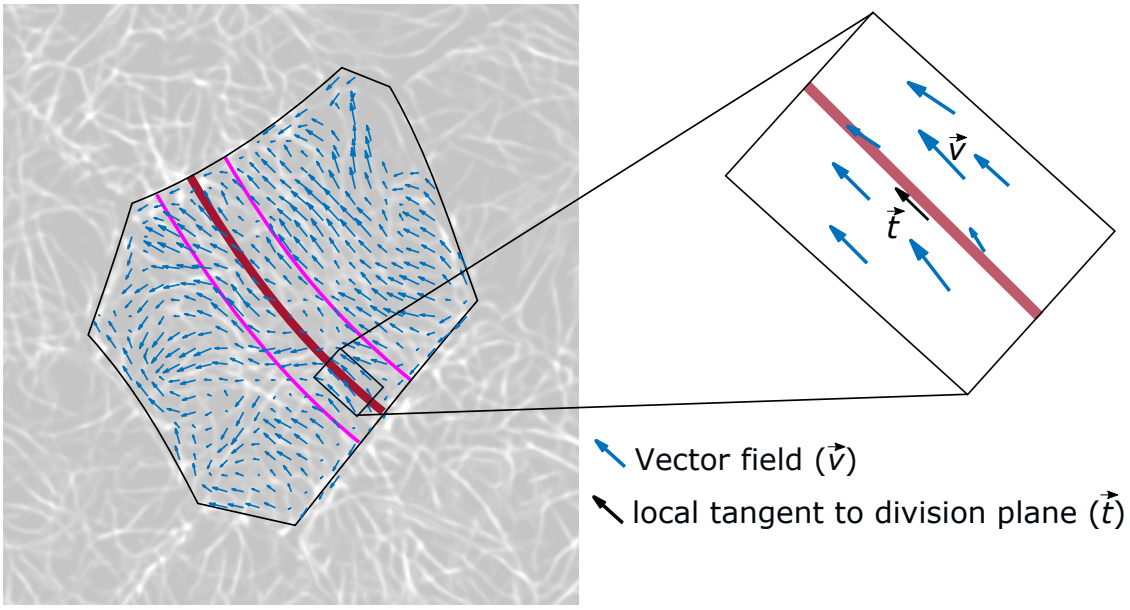

Figure 8: Analysis of microtubule alignment with the alternative division planes.

An area of 2µm of thickness around each alternative division plane was defined (magenta curves). Here, the shortest division plane is represented (brown). The vector field (blue arrows) shows the local orientation of MTs. For each vector inside of the magenta area, the inner angle was calculated between the vector ($\vec{v}$) and the tangent vector to division plane ($\vec{t}$) closest to the vector.

5.5.3 Microtubule orientation on the peripheral edge

We developed a MATLAB code to analyze a batch of images. Beside of the images, we used the vector fields and the cell contours (Section 5.4). We get the peripheral area eroding the cell contour. Each vector inside of the area were evaluated to get the inner angle with the closest tangent vector to division plane (Figure 20A).

5.5.4 Microtubule orientation around the vertex.

To analyze the MT orientation around the vertex we developed a MATLAB routine. We used the vector field, the cell contour and vertex coordinates from the MATLAB routine described in the section 5.4. We considered the peripheral area obtained in the section 5.5.3. The area around the vertex was established using 2µm from the vertex in the cell contour and the vertex in the eroded cell contour. The limited area around the vertex was subdivided into small rectangles and triangles to observe the change of distribution according to the distance from the vertex. The numbers of vectors by the small polygon generated were normalized by area (Figure 21A).

5.6 Algorithm for the simulation of microtubule dynamics.

We developed a model of microtubule dynamics implementing the two-state instability model in C++ following the approach of Dixit & Cyr (2004) (Figure 9). We used the dynamic instability parameters of MT published from experimental data; the growth and shrinking velocities of MTs (v_g, v_s), the catastrophe and rescue rates (r_c, r_r) and the rate of nucleation (r_n) (Dixit and Cyr, 2004; Drechsel et al., 1992; Howard, 2002; Hyman et al., 1992) (Table 1). The probabilities of MT-MT interaction have been estimated for the whole range of collision angles using the probability distribution determined by Tindemans, 2010, based on experimental data. The angle-dependent collision outcome probabilities P_{zip} (zippering), P_{cat} (induced catastrophe), and P_x (crossover) are assumed to be independent of the polarity of the microtubules and therefore are defined on the interval $[0, \frac{\pi}{2}]$:

$$P_{zip} = \frac{1-\cos(4\alpha)}{4\sin\alpha}, \tag{4}$$

$$P_{cat} = \frac{3-4cos(2\alpha)+cos(4\alpha)}{16sin\alpha}, \tag{5}$$

$$P_x = 1 - P_{cat} - P_{zip}. \tag{6}$$

When a MT reaches the cell border, it is stabilized for a duration $T = \tau_{\text{eff}} l_0 / v_0$, where $l_0 = (r_c / v_g - r_r / v_s)^{-1}$ is the mean length of non-interacting MTs and $v_0 = v_g v_s / (v_g + v_s$ the characteristic MT velocity. τ_{eff} is the effective boundary pause time (dimensionless), it was considered 0 when catastrophe is induced and it was considered 1 when the MT pause for 430s in the cell edge (Table 1).

The nucleation of MT at the border was simulated using a probability p to be nucleated randomly within the surface of the cell, and a probability $1-p$ to be nucleated randomly along the edge. MT are nucleated with an α angle of $90° \pm 5°$ with the border. We quantified MTs local orientation with respect to a direction defined by the angle α, by evaluating the quadrupole

$$S_{xy}(\alpha) = \int_0^{2\pi} \frac{1}{2}\left(3\cos^2(\theta-\alpha)-1\right) f_{xy}(\theta)\mathrm{d}\theta, \tag{7}$$

where $f_{xy}(\theta)$ is the normalized orientation profile at the location (x, y). When MTs are all perfectly aligned with the direction α, $S_{xy} = 1$, when MTs have random orientations,

$S_{\mathrm{xy}} = 0.25$, and when MTs are perpendicular to the direction α, $S_{\mathrm{xy}} = -0.5$. We calculate the average value of the product between the MT density and S over the whole surface area of the cell A,

$$\langle S \rangle = \frac{1}{A} \iint \hat{\rho}_{xy} S_{xy}(\alpha) \mathrm{d}A, \tag{8}$$

where $\hat{\rho}_{xy}$ is the normalized concentration at the location (x, y).

Parameter	Values/Function	Description
v_{g}	0.08 µm s^{-1}	Growing velocity
v_{s}	0.16 µm s^{-1}	Shrinking velocity
v_0	0.05 µm s^{-1}	Characteristic velocity
r_{c}	0.007 s^{-1}	Catastrophe rate
r_{r}	0.007 s^{-1}	Rescue rate
r_{b}	$\geq$ 0.001 s^{-1}	Boundary catastrophe rate
l_0	22.85 µm	MT natural length
τ_{eff}	$\frac{v_{\mathrm{c}}}{l_0 r_{\mathrm{b}}}$	Normalized boundary pause time

Table 1: Parameters for the MT dynamics used in the biophysical model (based on Tindemans, 2010).

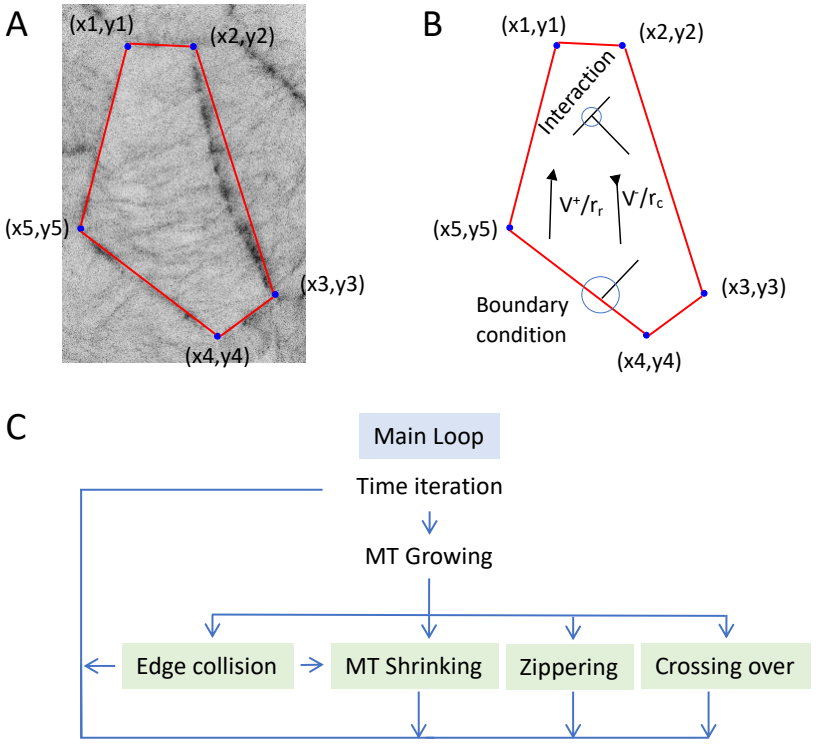

Figure 9: Scheme for the biophysical model developed in C++.

A, Raw image used to extract the cell shapes. The cell geometry is the input for the algorithm. **B,** Dynamic parameters of MTs; Interaction between MTs, boundary condition and dynamic instability parameters. **C,** At the beginning of the algorithm, several microtubules are nucleated with random orientation. During the growing state, the MTs can continue growing or change their state to shrinking, interact with other MTs or start a pause state when reaching the cell border. This process is an iterative process that depends on the time of simulation used, which is considered in seconds.

6. RESULTS

This section contains the results organized by each specific objective proposed for this thesis (see section 4). The first specific objective, which is quantify the spatial distribution of microtubules in cells undergoing division, will be presented in four subsections in accord with the main analyzes. First, we tested the cell division rule in a broad set of cell geometries in *Marchantia* cells. Second, we analyzed the microtubules organization in early interphase and during the preprophase formation in order to correlate it with the geometrical cell division rule. Third, we quantified the local orientation of MTs along the cell edges to study weather the cell border can influence locally the MT distribution, and fourth, we tracked the MTs along the cell edge to observe the dynamic among periclinal and anticlinal faces. The results obtained in the second and third objectives will be presented in the section 6.2 and 6.3, respectively.

6.1 Distribution of microtubules in cells undergoing division.

We are testing the hypothesis that **microtubule dynamics and the interaction of microtubules with the cell edges are sufficient to explain the positioning of the PPB in least-area configurations**. The self-organization allows the formation of mitotic spindles and asters during cell division and it is also proposed as a process behind of the PPB formation in a defined orientation (Besson and Dumais, 2011; Dhonukshe and Gadella, 2003; Karsenti, 2008; Vos et al., 2004). Several studies have demonstrated that the MTs are able to respond to the cell shape (Ehrhardt and

Shaw, 2006; Granger and Cyr, 2001; Sugimoto et al., 2000; Thoms et al., 2018). However, to date, the transition between the MTs in interphase and the PPB has not been studied, therefore, in this objective, we studied the distribution of microtubules in cells undergoing division. As a first step, we tested the cell division rule in *Marchantia* cells. As a second step, we analyzed the MTs orientation during stages of interphase to correlate with the division plane predicted by the cell division rule. Finally, we analyzed the local MTs orientation on the periclinal face during the PPB formation, including dynamic analysis.

6.1.1 *Marchantia polymorpha* cells follow the geometrical cell division rule.

It is expected the positioning of the division plane results from a competition between alternative configurations whose geometries represent local area minima (Besson and Dumais, 2011). To test the division rule, we generated an image dataset of 340 recently divided cells. We used a recombinant line expressing the membrane protein Lit6b, which is fused to the fluorescence protein mCitrine (reporter gene). This reporter is under the control of a promoter expressed in meristematic cells. This line was developed and provided by the team of Dr. Jim Haseloff (Cambridge University). We used this line to follow the new division plane over time (Figure 10).

Gemmae were isolated to observe the notch using confocal microscopy. We tracked division plane formation in 340 cells. The images were analyzed to capture the vertices and edges of the cell (Figures 11). Based on this geometry, the division planes were predicted using a MATLAB algorithm developed by Besson and Dumais, 2011. For each cell, we predicted the four shortest division planes following the

geometrical cell division rule. We compared the observed and predicted division planes in order to classify each observed division plane as the shortest, second shortest, third shortest and fourth shortest (Figure 12A). We found that 78.8% of the cells divide following the shortest division plane, while 15.9%, 4.12% and 0.29% of the cells divide following the second, third and fourth shortest division planes, respectively (Figure 12B). The division plane frequencies recorded for *Marchantia* are similar to those previously reported for *Zinnia elegans* and *Microsorum punctatum* (Besson and Dumais, 2011).

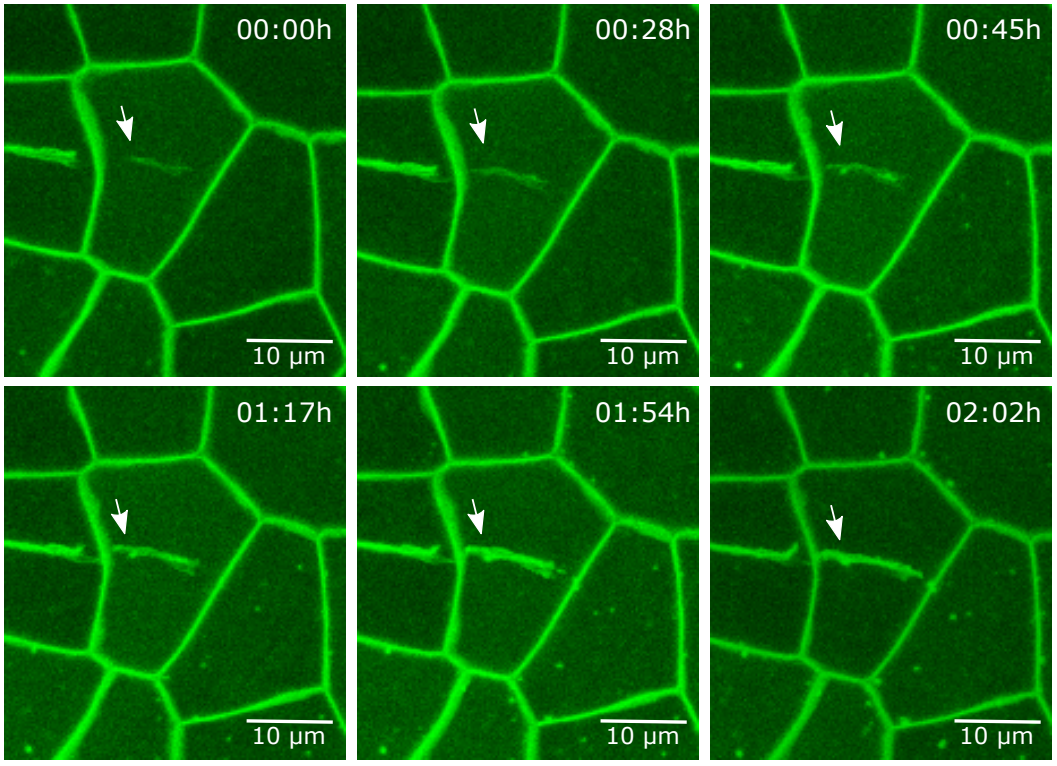

Figure 10: Time lapse of division plane formation in meristematic cell of Lit6b-mCitrin line of *Marchantia polymorpha*.

The time sequence shows the formation of the new division plane (white arrow).

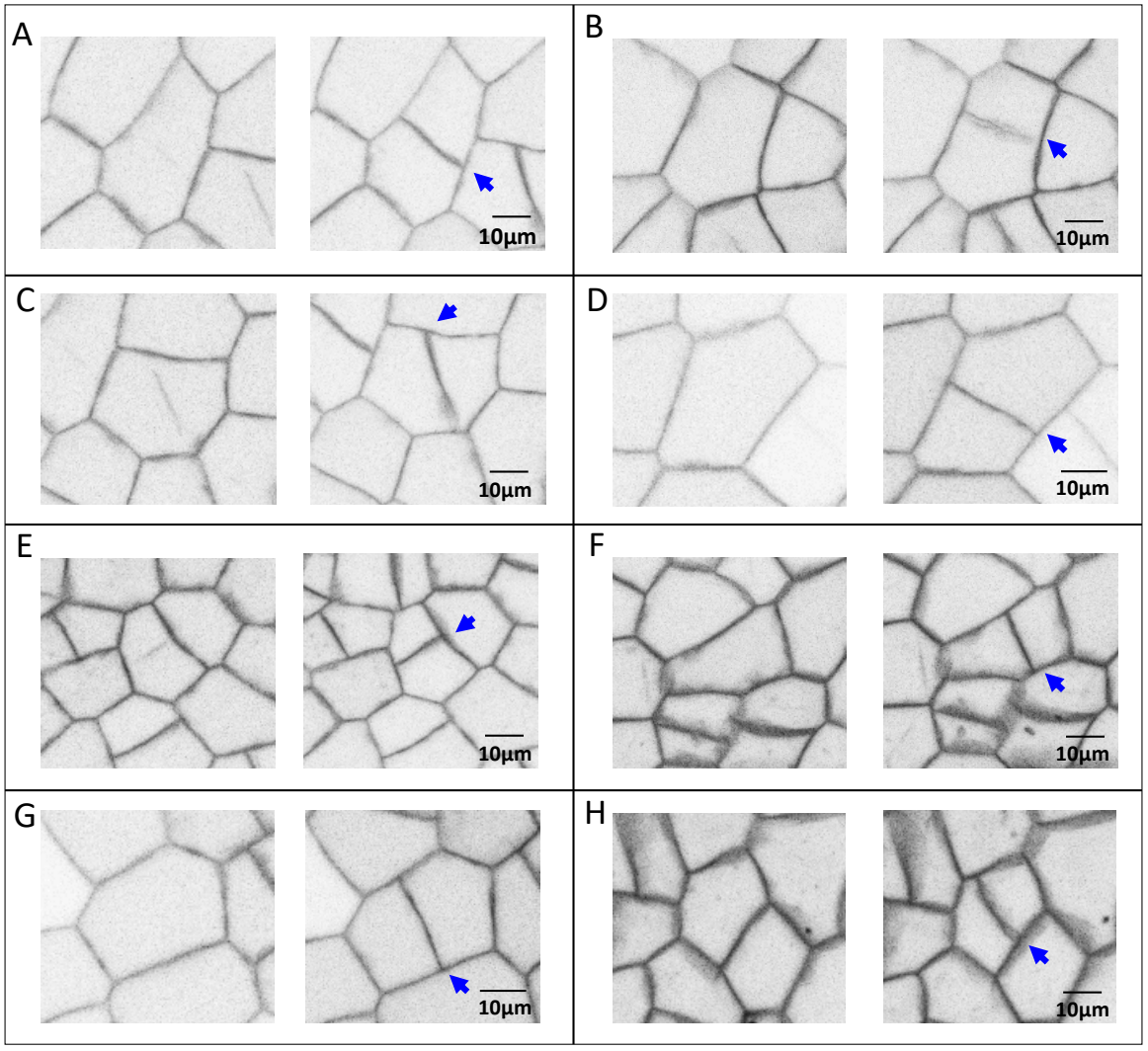

Figure 11: A selection of meristematic cells before and after division in the Lit6b-mCitrin line of *Marchantia polymorpha*.

A-H, Blue arrows indicate the new division plane. A total of 340 new division planes were observed.

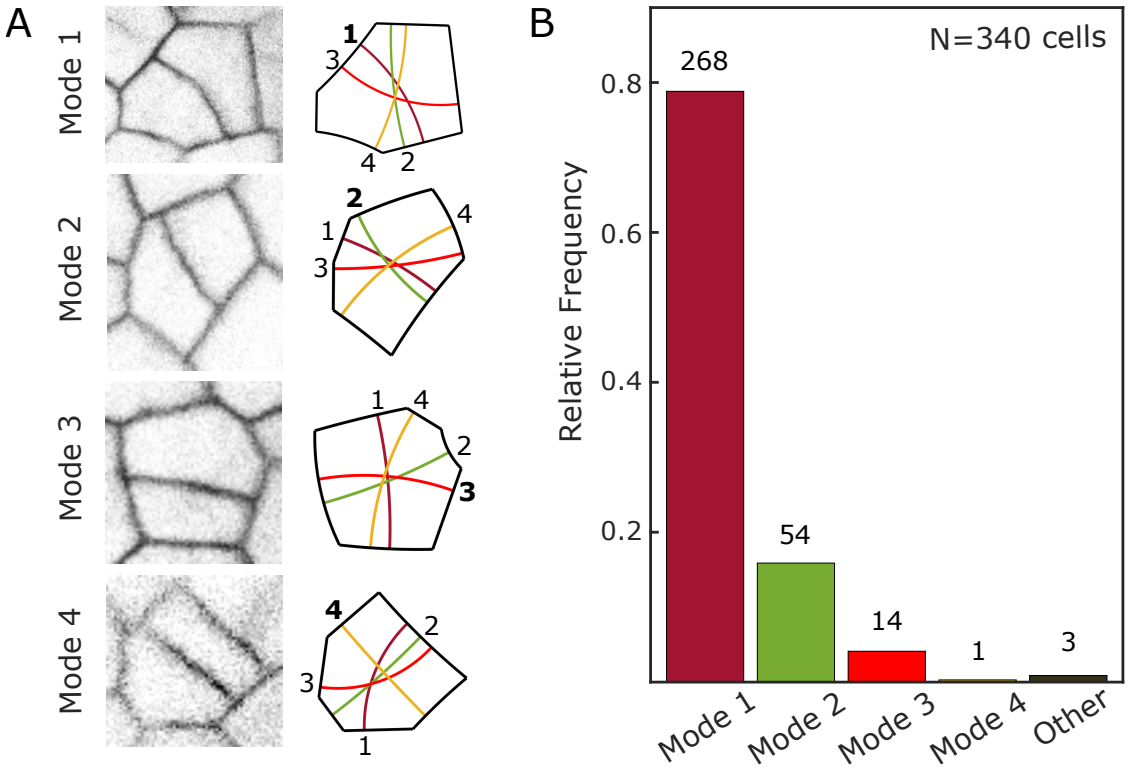

Figure 12: Selection of the division plane in *Marchantia polymorpha* cells.

A, Recently divided notch cells (left) and the four shortest division planes predicted for the cell shapes (right). The cells are examples of divisions along the shortest (mode 1), second shortest (mode 2), third shortest (mode 3), and fourth shortest (mode 4) planes. **B**, Frequency of the different division modes for the notch cells. Overall, 78.8%, 15.9%, 4.1%, 0.3% and 0.8% of the cells divide along the shortest plane, second shortest, third shortest, fourth shortest and others, respectively.

The probability of observing a particular division plane among two competing planes i and j is given by the Gibbs measure (Eq. 1). To compute the distributions, we chose the cells dividing along the shortest (i) and second shortest (j) division planes. We calculated the probability of choosing the shortest division plane (i) for a range of δ_{ij} (from 0 to 0.5 with intervals of 0.06), where δ_{ij} is the relative length difference between planes i and j.

The results show that cells with $\delta_{ij} \leq 0.2$, which represent small length difference,

were more likely to divide along non-shortest paths than cells with $\delta_{ij} > 0.2$ as expected. To evaluate the similarity between Besson and Dumais model and our experimental observation, we fit the distribution to the exponential model given in Gibbs measure and we obtained the β parameter for *Marchantia*. The parameter β captures the mechanism behind the selection of the division plane. A large β value indicates that cells can select the shortest division plane reliably. A low β value means that each alternative division plane has the same probability of being selected. We found that our experimental observations are related to the probabilities predicted for all the biological systems compared. The β parameter calculated for *Marchantia* was 19.4, which means that cortical MTs are strongly responsive to cell geometry. This value is identical to the one calculated for *Coleochate*, that share the same closest ancestor as *Marchantia* (Figure 13). Moreover, the β value is similar to the one obtained for angiosperms (a mean of 20.8) and ferns (20.5). Therefore the probability to observe non-shortest paths depend on the relative length between competing division planes, which is in agreement with the cell division rule.

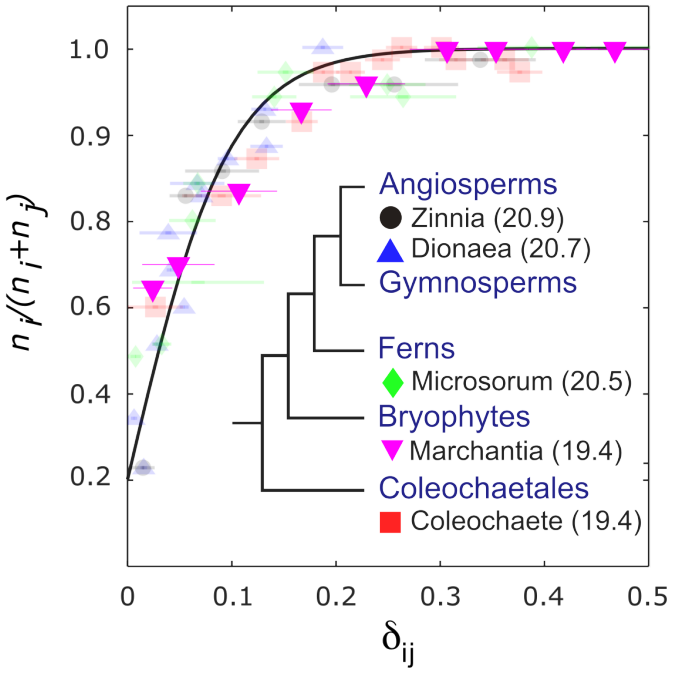

Figure 13: Universal rule for the selection of the plane of division.

The plot shows the proportion of cell divisions along plane i (y-axis) as a function of the relative length difference to plane j (x-axis). δ_{ij} calculated from our analysis of *Marchantia* is showed in magenta inverted triangles. Different species previously published were represented as opalescent data (Besson and Dumais, 2011). The solid line is the best fit of the experimental data with the equation $[1+e^{\beta\delta_{ij}}]^{-1}$. The β value for *Marchantia*, obtained from our dataset, is 19.4.

6.1.2 The orientation of the interphase microtubules follows the cell division rule.

The cell division of hepatic mosses, such as *Marchantia*, show differences with land plants. The hepatics show so-called polar organizers when preparing for cell division, which are centrosome-like microtubule organizing centres localized to opposite ends of the preprophase nucleus (Fowke and Pickett-Heaps, 1978). Polar organizers appear before that the preprophase band is formed, when the cortical MTs are around the cell surface. Therefore, we used this characteristic as a cell cycle marker

that allow us choose and follow the cells starting the PPB formation (Figure 14).

The location and orientation of PPB define the future division plane, as demonstrated in the 60's for several species (Buschmann et al., 2016; Pickett-Heaps and Northcote, 1966; Rasmussen et al., 2011, 2013). We tested this relation in *Marchantia* cells, where we merge the signal of MT forming the PPB and the cortical MT signal around the new division plane. Our observations demonstrate that the PPB is coincident with the new cell division plane (Figure 15).

Before forming the PPB, cortical microtubules in the interphase form an aligned array perpendicular to the growth axis. The microtubule orientation in the PPB is inherited from the cortical array in interphase, suggesting that the orientation of PPB could be determined during late G2 in interphase (Cleary et al., 1992; Vos et al., 2004). However, this relation has not been demonstrated. Thus, we get a large group of images of microtubules in interphase of highly proliferative cells to analyze the interphase MT distribution and its relation with the cell shape.

We obtained an image dataset of 105 cells in interphase with the microtubule signal. The global orientation of each cell was obtained using a plugin in FIJI: FibrilTool. This software is widely used to measure the orientation of microtubules (Boudaoud et al., 2014). Moreover, we used the MATLAB algorithm from Besson and Dumais to obtain a dataset of the vertices describing the cell shape and the alternatives prediction planes. The global MTs orientation was obtained and compared with the closest alternative division planes orientation, obtaining 50%, 22.2%, 13.3% and 11.1% of the cells aligning the MTs along the shortest plane, second shortest, third shortest and fourth shortest, respectively. This result showed a similar distribution to the cell

division rule (Figure 16).

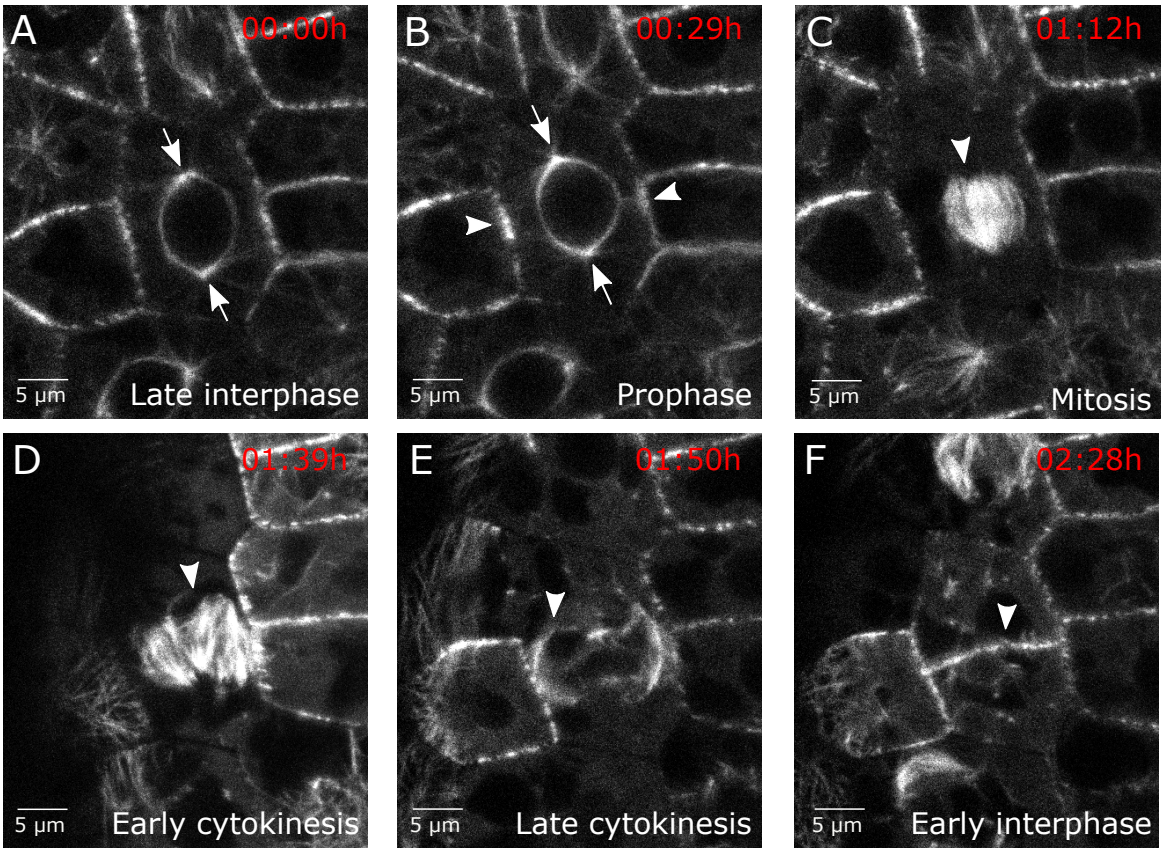

Figure 14: Cytoskeletal organization in dividing plant cells of *Marchantia polymorpha*.

The panel is based on expression of GFP-tubulin in cells of *Marchantia*. **A-B**, During the late interphase start the formation of the polar organizers (white arrows), structures that are formed previous to the PPB and are maintained until the PPB is formed (white arrowheads in B). Therefore, the polar organizers can be used as a cell cycle marker that allow anticipate the PPB formation. **C**, After nuclear envelope and PPB breakdown a metaphase spindle is formed. **D-E**, Subsequently, during the cytokinesis, the phragmoplast is formed to guide the deposition of components to the new cell wall. **F**, After completion of cytokinesis microtubules populate the new cross wall (white arrowhead).

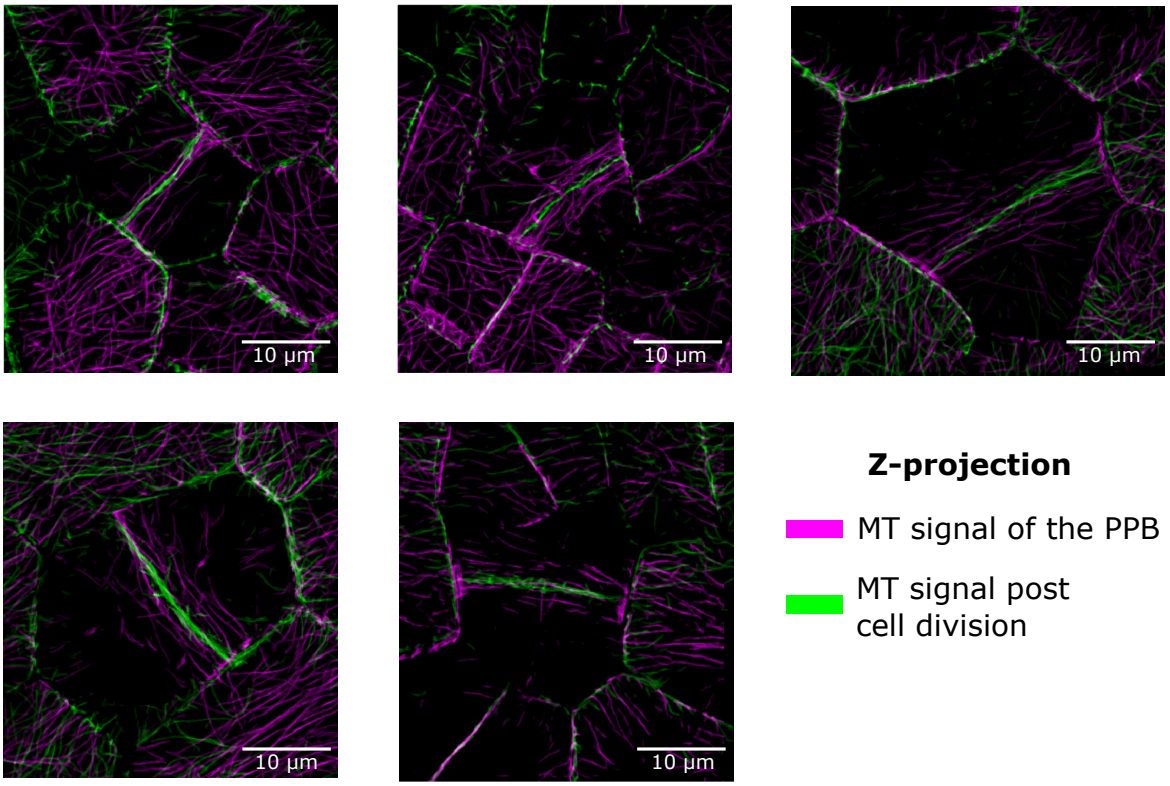

Figure 15: Similarity in orientation among the position of division plane and preprophase band in *Marchantia polymorpha* cells.

Z-projection of MTs signal in cells of tubulin-GFP line of *M. polymorpha*. The images were acquired in two times of the cell cycle; when the PPB is formed and after that new plane is formed (after cell division). Merge of PPB (magenta) and division plane (green) in five cells.

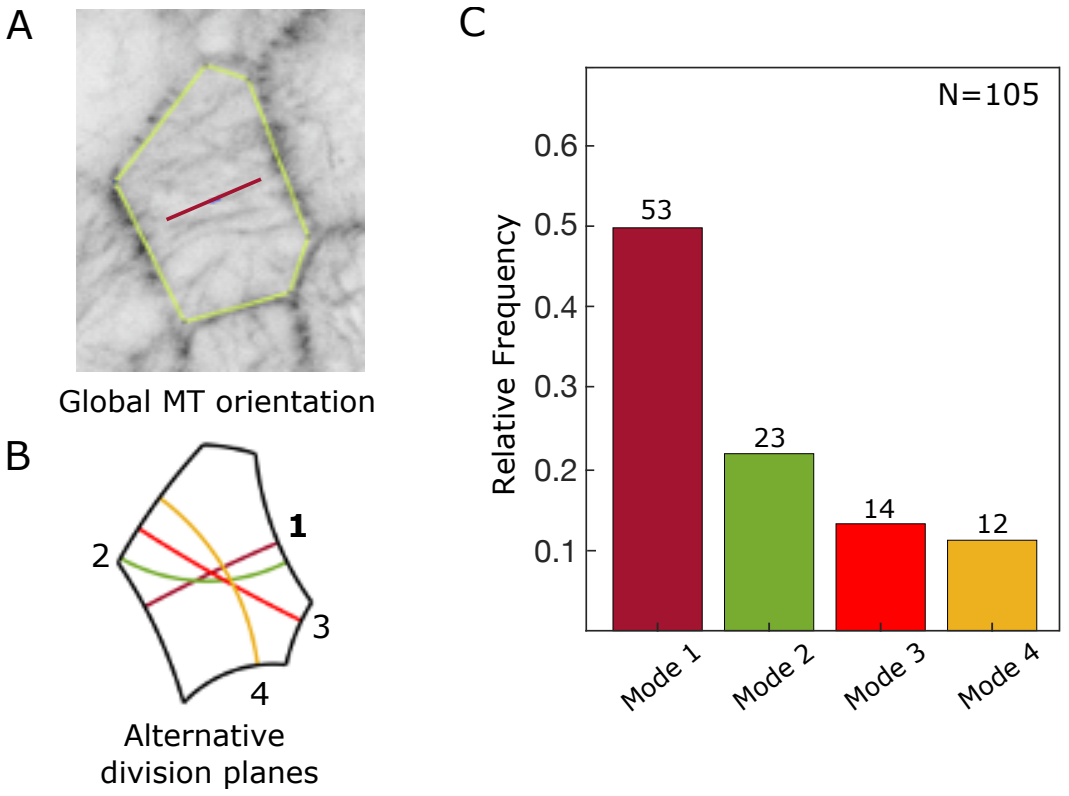

Figure 16: Microtubule organization in interphase follows the cell division rule.

A, Microtubule distribution in interphase of 105 cells was analyzed using the Fiji plugin, FibrilTool. **B**, Alternatives division planes were predicted for each cell shape using the code published by Besson and Dumais, 2011. **C**, MTs orientation was compared with each alternative division plane (mode) and classified in a mode respect to the closeness. Then, the relative frequency obtained was 50%, 22.2%, 13.3% and 11.1% of the cells aligning the MTs along the shortest plane, second shortest, third shortest and fourth shortest, respectively.

Based on our observations we proposed a mechanism of the MT self-organization to form the PPB. This mechanism could start with a local alignment, which would favor the formation of a first bundle that cause catastrophe events in MTs that are in an orthogonal orientation and cause the zippering of MTs aligned with this first bundle. Considering the geometrical division rule, the first bundle (nascent PPB) could be oriented in the direction of any alternative division plane predicted for the given cell shape. To test the mechanism that we propose we get a dataset of time-lapses

tracking the PPB formation, starting with cortical MTs uniformly distributed on the periclinal face (Figure 17). We defined an area around the alternative division planes predicted (Figure 18A, Figure 19A,). On that area we quantified the local MT orientation and its alignment with the division plane (see section 5.5.2, Eqs. 2,3). The alignment measure, $Projection$, has a value of 1 when MT and division plane are parallel and -1 when they are perpendicular.

We analyzed the start and the end points of 48 time-lapses acquired. We obtained a histogram where each cell was classified as mode 1,2,3 or 4 based on the alignment of the MTs along the division plane. In the beginning of the PPB formation we found that 28% of the cells have a maximum alignment in the mode 1, 17.6% in the mode 2, 39.7% in the mode 3 and 14.7% in the mode 4 (Figure 18B).

To get the distribution of Gibbs we compared two alternatives division planes, i and j, where the length of plane i is shorter than length of plane j. The Gibbs measure was calculated using the Eq. 1, where n_i and n_j are the number of cells that have a maximum alignment along the plane i and j, respectively.

We average the Gibbs measure for a range of δ_{ij} (from 0 to 0.4 with intervals of 0.04). The results showed the probability for MTs to align following the alternative division plane predicted, which is different to what was observed when the geometrical rule was evaluated (Figure 18C). The β value obtained by the interpolation of the function written in Eq. 1 was 0.5. This low value of β indicates that the MTs distribution in this stage of the cell cycle do not follow the cell division rule.

To evaluate the cell division rule in this dataset of 48 cells, we analyzed the MT

orientation around the alternative division planes in the end time points of the time-lapses, when the PPB is formed. The results showed that 62.5% of the cells have a maximum alignment in the mode 1, 20.8% in the mode 2, 14.6% in the mode 3 and 2.1% in the mode 4 (Figure 19B). Those results have same bias of the geometrical division rule, however, they have differences in the relative frequency of each mode. In relation to this result, the distribution of Gibbs measure showed that with $\delta_{ij} > 0.15$, the cells were more likely to align the MTs to the shortest paths (Figure 19C). Nevertheless, we get a β value of 10.5, which is lower that we obtained for our model, 19.4 (Figure 13).

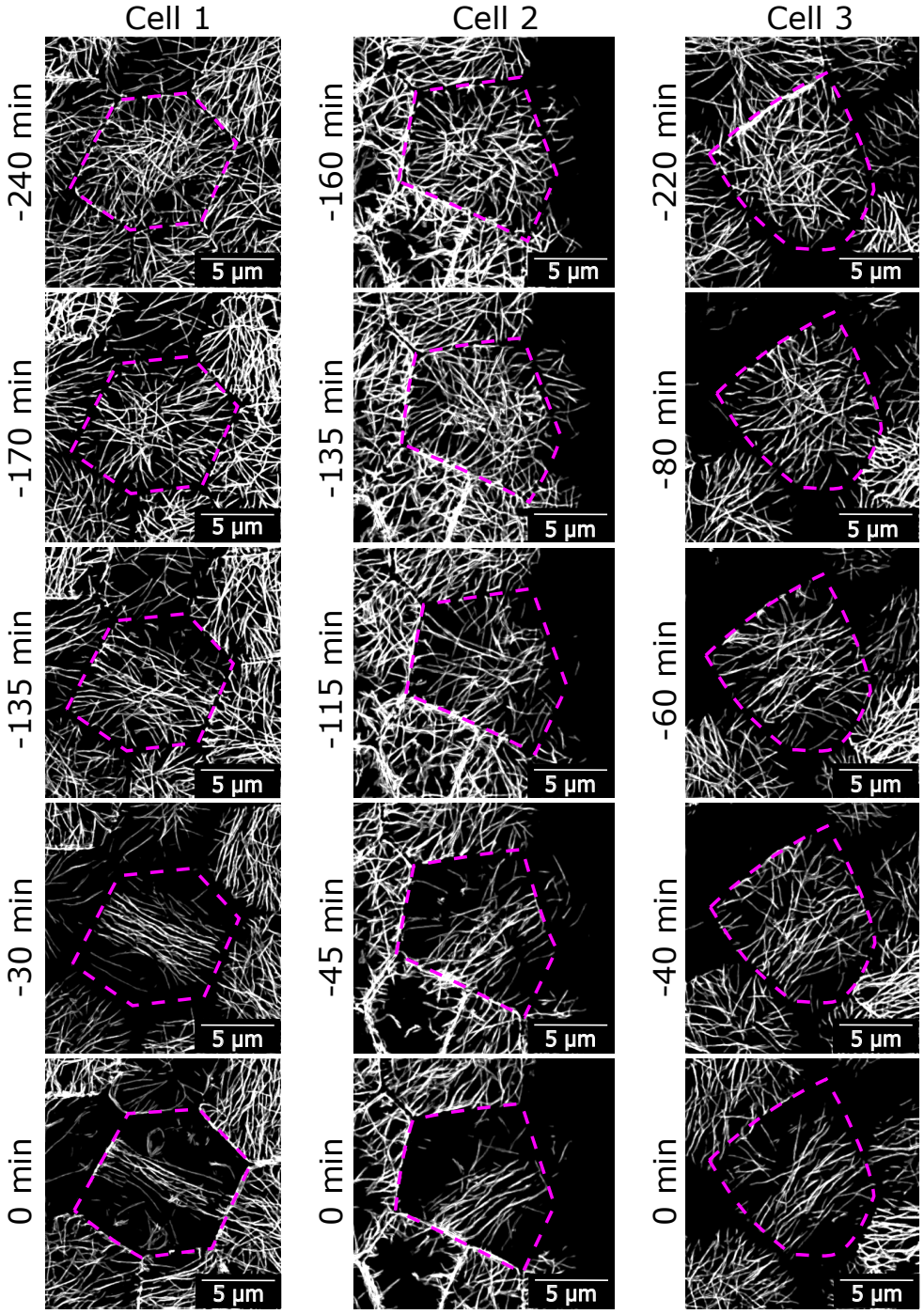

Figure 17: Subset of dataset of the preprophase band formation time lapses shows the organization of microtubules during this process.

The panel show three representative cells out of 130 cells that were followed during the PPB formation. The Z-stack of each image was filtered and projected. Magenta dashed line draws the contour of the cells. Five time points were selected from the total time points. When the PPB is formed, the time is considered 0 min.

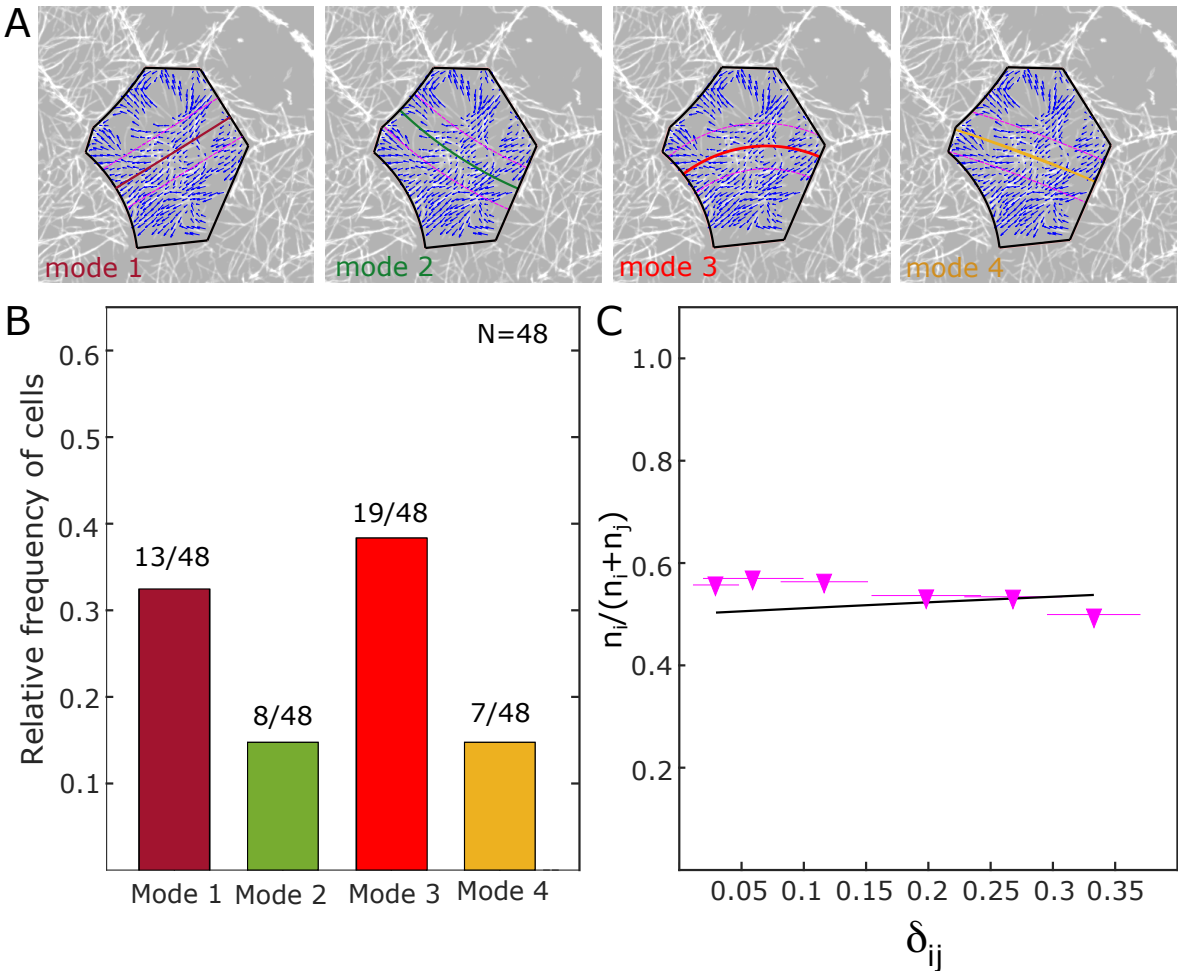

Figure 18: Microtubule alignment along the alternatives division plane during late interphase.

A, Representation of the area around the four shortest alternatives division planes analyzed. The area is limited by magenta lines. The microscopy image analyzed represent the start point of the time lapse. **B,** Relative frequency of the number of cells that have the maximum alignment along the mode 1, 2, 3 or 4. **C,** The plot shows the proportion of MT projections along plane i as a function of the relative length difference to plane j, δ_{ij} ($l_i < l_j$,). $N = 48$ cells.

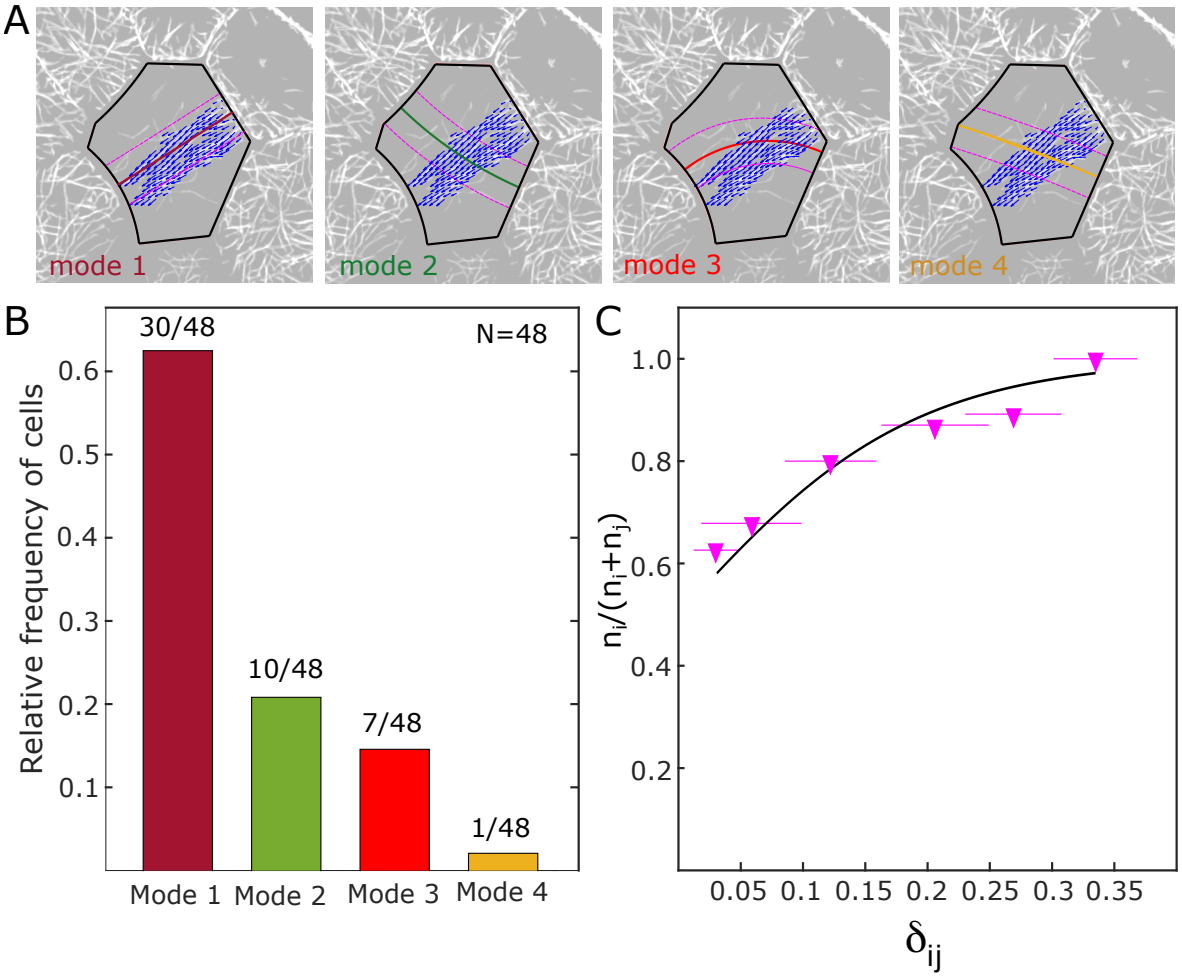

Figure 19: Microtubule alignment along the alternatives division plane during late prophase.

A, Representation of the area around the four shortest alternatives division planes analyzed. The area is limited by magenta lines. The microscopy image analyzed represent the end point of the time lapse. **B**, Relative frequency of the number of cells that have the maximum alignment along the mode 1, 2, 3 or 4. **C**, The plot shows the proportion of MT projections along plane i as a function of the relative length difference to plane j, δ_{ij} $(l_i < l_j,)$. $N = 48$ cells.

6.1.3 Microtubules at the cell border are oriented orthogonal to the cell edge.

Based on our observation of the time-lapses acquired during the PPB formation, we noticed that the cortical MTs near the edge are oriented orthogonal with respect to the edge tangent. We used the vector field of MT orientation to analyze the MT signal corresponding to the peripheral area of the periclinal face. The peripheral area obtained by those contours is subdivided into smaller rectangles and triangles to evaluate in each one the average orientation of the vectors with respect to the edge tangent. We analyzed our dataset considering all cells and times, and we obtained a histogram of MTs angle distribution on the peripheral area relative to the edge tangent. We found that the MTs are oriented mainly orthogonal to the edge, which suggests that the cell edges influence the average orientation of MTs in that zone (Figure 20). The orthogonal distribution could cause that MTs compete among each other in the sharp vertices (cell corners), which would be reflected in the distribution of MTs around each vertex. We analyzed a total of 2302 areas around vertices; those were subdivided into small rectangles and triangles to observe the change of distribution relative to the distance from the vertex. We found that the MTs density was increasing while the distance from the vertex was also increasing (Figure 21).

To evaluate if there is a continuity between the MTs in the periphery of the periclinal face and the anticlinal face, we compared the MT orientation on both faces. We visualized the stack as a 3D volume using the Fiji plugin 3D Viewer (Figure 22A). Moreover, we projected the anticlinal (xz planes) and periclinal (xy planes) MTs signal, both projections were put together to check the continuity (Figure 22B). We

analyzed 313 MTs distributed on 25 edges, and we found that 63% of the MTs have continuity between the two faces, 25.5% of the MTs are in the anticlinal face and do not have continuity to the periclinal face, and 10.5% of the MTs are in the periclinal face and do not have continuity to the anticlinal face (Figure 22C). The orientation of the MTs on both faces showed an orthogonal orientation relative to the cell edge (Figure 22D). Therefore, a high percentage of the MTs cross the edges to continue to the next face keeping the same orientation.

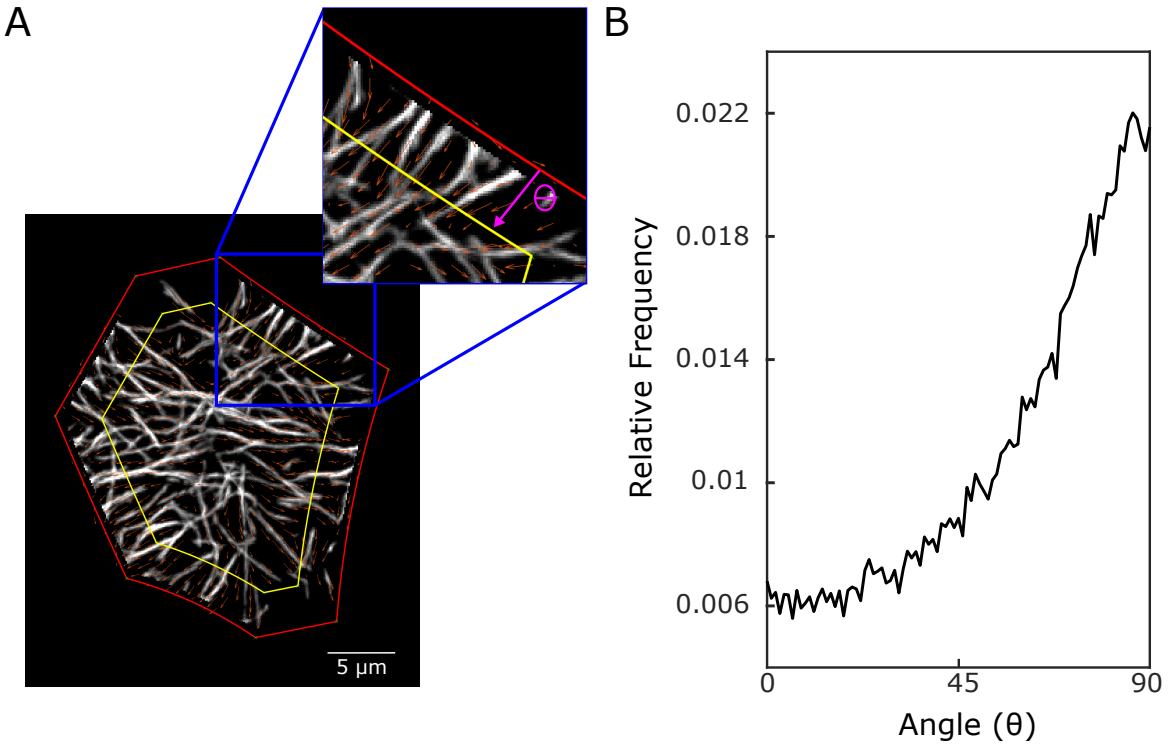

Figure 20: Peripheral microtubules on the periclinal face are oriented in orthogonal direction relative to the cell edge orientation.

A, The cell contour is defined by the red polygon. The red polygon and the smaller yellow polygon is drawn to define the cell border. The MTs orientation (θ) in the cell border was measure relative to the cell edge orientation. A MT orthogonal to the cell edge is represented by the magenta arrow. **B**, The histogram represents the probability of each angle in the local orientations analyzed. The result corresponds to 50 cells analyzed that include 62.102 local orientations (vectors).

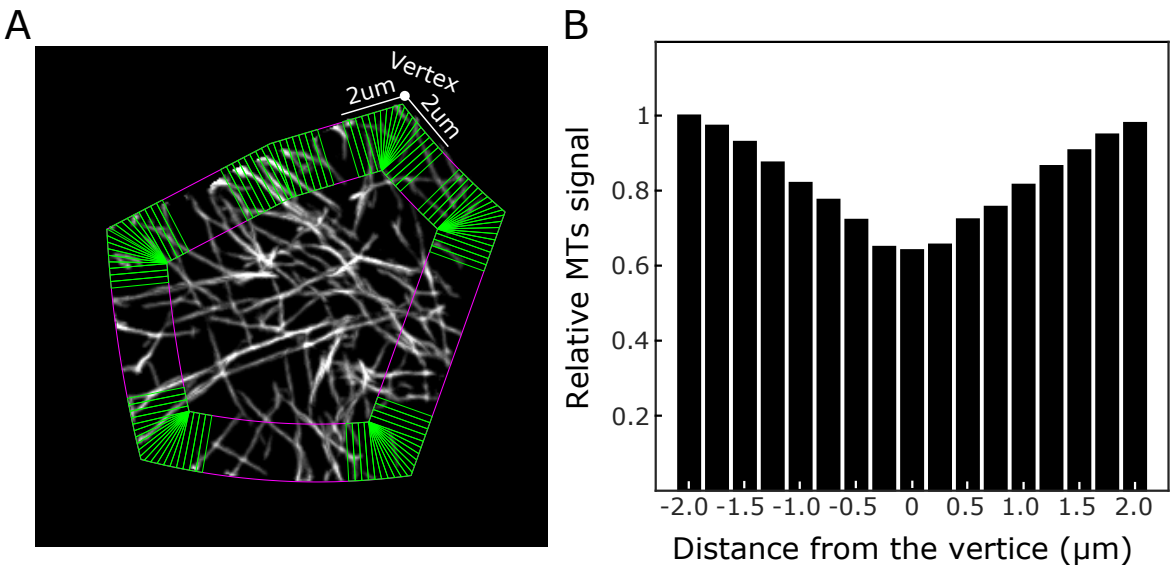

Figure 21: The microtubule signal is decreased in the vertex area.

A, The distance from the vertex was $2\mu m$, and the area considered include the peripheral zone on the periclinal face around the vertex. Each area was subdivided into triangles and rectangles (green), and the MT signal was quantified. **B**, Relative frequency of MTs signal along the small zones (triangles and rectangles) around the vertex. The MTs signal in each small zone was normalized by area and by the total of vertices analyzed. $N = 2.302$.

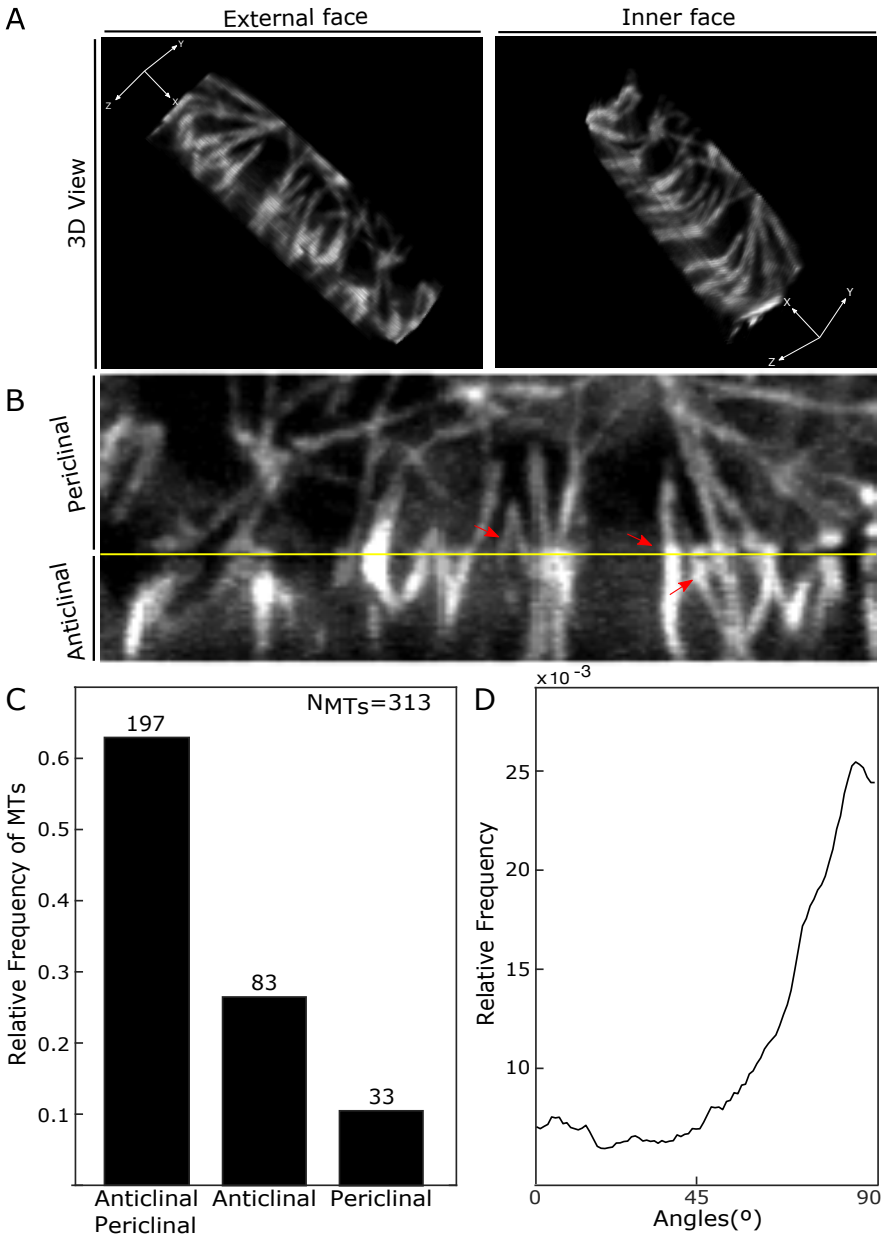

Figure 22: Microtubules continuity between anticlinal and periclinal faces.

A, 3D visualization of anticlinal and periclinal MTs in a *M. polymorpha* cells. **B**, xz and xy projection, which represent the anticlinal and periclinal MTs, respectively. The upper red arrow show two MTs from the periclinal without entering to the anticlinal face. The middle red arrow show a MT with continuity among both faces. The bottom red arrow shows a MT from the anticlinal face without entering to the periclinal face. **C**, Relative frequencies of the events showed in B, a total of 313 MTs were quantified. **D**, MT orientation relative to cell edge on both faces.

6.1.4 Microtubules going from the anticlinal face to the periclinal face .

In the previous section we observed that the MTs are mostly oriented orthogonal to the cell edges between the anticlinal and periclinal faces. The MT direction indicates how the MTs interact in the periclinal face and thus help to understand the MT dynamics during the PPB formation. Therefore, we analyzed time lapses images from spinning disk microscopy to analyze the MT direction near the edges. We get time lapses on five edges of different cells and we counted the number of MTs growing toward the anticlinal or periclinal face. We found that 68.3% of MTs are growing toward the periclinal face and 31.7% are growing toward the anticlinal face (Figure 23). Those proportions are similar to the ratio among anticlinal and periclinal MTs observed in the continuity study described in the previous section (Figure 22C).

Additionally, we extracted growing and shrinking velocities, which are part of the dynamic parameter describing the dynamic instability of MTs. Kymographs were generated for every MT in shrinking and growing events. The rate was determined by calculating the ratio between the MT length and time obtained from the kymographs. The shrinking and growing rate obtained was $0.13\,\mu m\,s^{-1}$ and $0.06\,\mu m\,s^{-1}$, respectively (Figure 24).

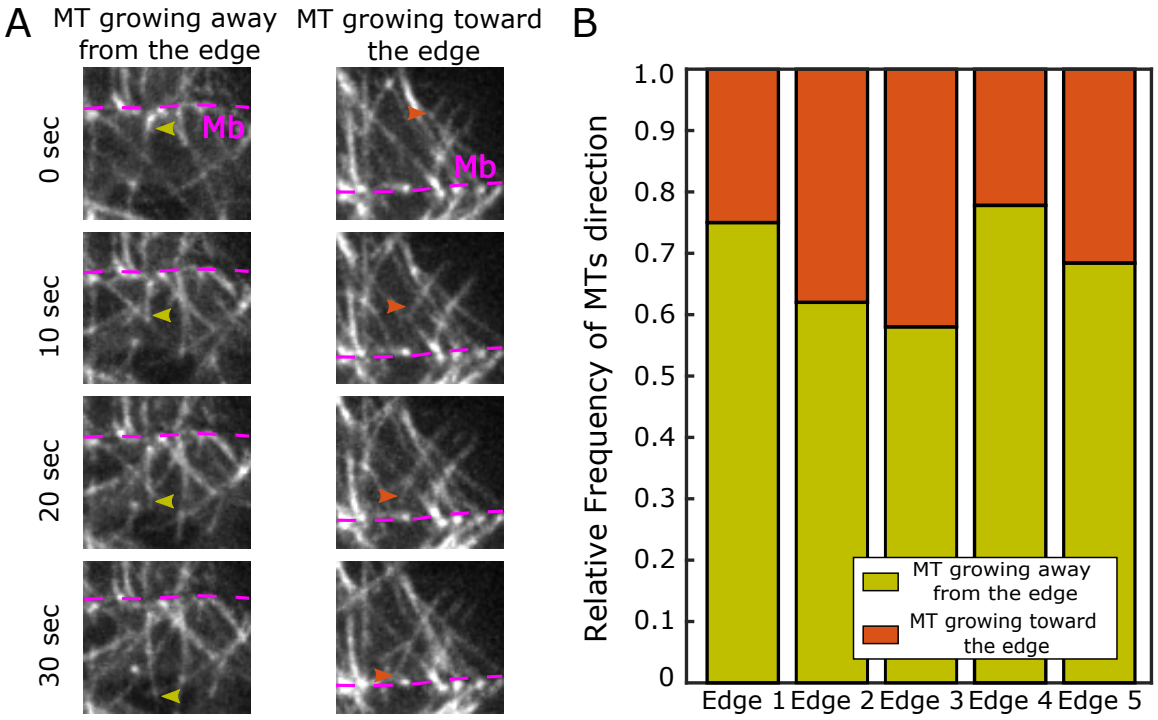

Figure 23: Microtubules at the border of the periclinal face come mostly from the anticlinal face.

A, The time lapses analysis of the MT dynamic in the border of the periclinal face was analyzed to detect MT direction around the edge area. The direction was represented for MTs growing away from or toward to the edge cell, mustard and orange arrows, respectively. Magenta dashed line indicate the cell edge. **B**, Relative frequency for each MT event was obtained. $N_{Edge\,1} = 91$, $N_{Edge\,2} = 39$, $N_{Edge\,3} = 56$, $N_{Edge\,4} = 36$ and $N_{Edge\,5} = 38$.

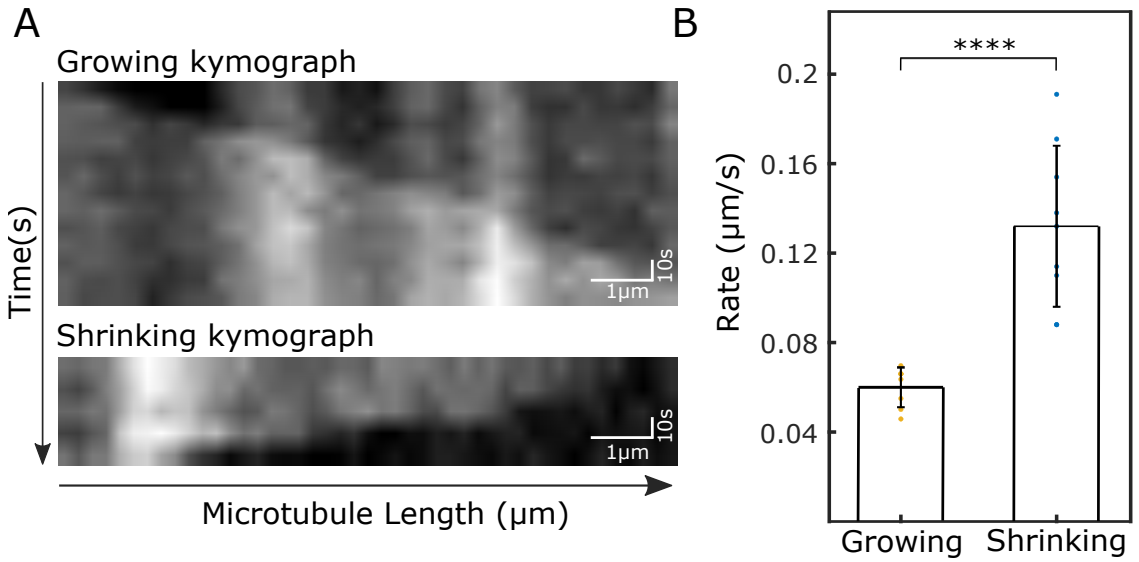

Figure 24: Average microtubule growth and shrinking velocity obtained during interphase.

A, Kymographs used to analyze the growing and shrinking rates. **B**, The mean velocity for growth was $0.06\,\mu\text{ms}^{-1}$ ($N = 8$) with a standard deviation of 0.009. The mean velocity for shrinking was $0.132\,\mu\text{ms}^{-1}$ ($N = 9$) with a standard deviation of 0.036. Results were statistically compared using two-tailed t-test. (****:$p < 0.0001$).

6.2 Biophysical model of microtubule dynamics and cell border interactions during the preprophase band formation.

We proposed in our hypothesis that microtubule dynamics and the interaction of microtubules with the cell edges are sufficient to explain the PPB formation in least-area configurations. To test whether these properties itself, without other molecular interactions, can sense the cell shape, we implemented a biophysical model where we simulated the dynamic of MTs in a surface. We developed a model of microtubule dynamics in C++ based on the two-state instability model of Dixit & Cyr (2004). In our model, we considered a realistic cell shape using dataset of vertices obtained previously with the MATLAB algorithm. On the surface simulated, every MT

is initiated by nucleating it at random position and random orientation over the surface, while its plus-end alternates between growing and shrinking states, which the MT respectively grows with a velocity $v_g = 0.08\,\mu m s^{-1}$ or shrinks with a velocity $v_s = 2v_g$ (Table 1). MTs switch from the growing to the shrinking state at a frequency given by the catastrophe rate, $r_c = 0.07 s^{-1}$, and from the shrinking state to the growing state at a frequency given by the rescue rate, $r_r = 0.07 s^{-1}$. A MT-MT interaction occurs when a growing MT encounters a barrier MT and has three possible outcomes: either the growing MT crosses the barrier, either it zips along the barrier MT, or either it undergoes a catastrophic event and start shrinking. The respective probability of each event depends on the incident angle (Tindemans et al., 2010). Finally, we modeled the effective MT stabilization at the edges using a pause time at the boundary, τ_{eff}, and it was considered 0 when catastrophe is induced and it was considered 1 when the MT pause for $430 s$ in the cell edge (Table 1).

The simulation using $\tau_{eff} = 0.0$ lead the microtubules oriented principally along to the long axis of the cell. Unlike, the simulation using $\tau_{eff} = 1.0$ lead to the MTs oriented along of the short axis (Figure 25A-C).

To compare our biophysical model with the experimental observation, we compared the global orientation of the MTs at the end of the simulation with the global orientation obtained in the interphase cell with the Fiji plugin, FibrilTool (Figure 25D). We found that the orientation obtained from FibrilTool is coincident with the range of angles with high frequency (Figure 25E). Therefore, using the parameters dynamic of MTs and boundary conditions, we could reproduce the distribution of the MTs array in interphase. Thus, the next question was to understand how the MTs could re-organize

from an array to form a PPB.

Based on our experimental observations, the MTs at the edge are coming mainly from the anticlinal face with an orthogonal orientation with respect to the edge. Therefore, we included this on a 2D simulation in a hexagonal shape, nucleating each MTs with a probability p to be nucleated randomly within the surface of the cell, and a probability $1-p$ to be nucleated randomly along the edge, with $p=0.75$. The MT was simulated with an angle $\sim 90° \pm 5°$ with the border. There are 3 main directions within the cell, the vertical direction ($\alpha = 90°$), and two ”diagonal” oriented respectively $\alpha = 30°$ and $\alpha = 150°$. We quantified MTs local orientation with respect to a direction defined by the angle α with a $p=0.75$, by evaluating the S value described in Eq. 8. When MTs are all perfectly aligned with the direction α, $S_{\text{xy}} = 1$, when MTs have random orientations, $S_{xy} = 0.25$, and when MTs are perpendicular to the direction α, $S_{\text{xy}} = -0.5$. Simulations showed a predominant alignment in one of the three directions and transition from one alignment to another (Figure 26A). Also, the density profile after the simulation time showed a PPB formation (Figure 26B).

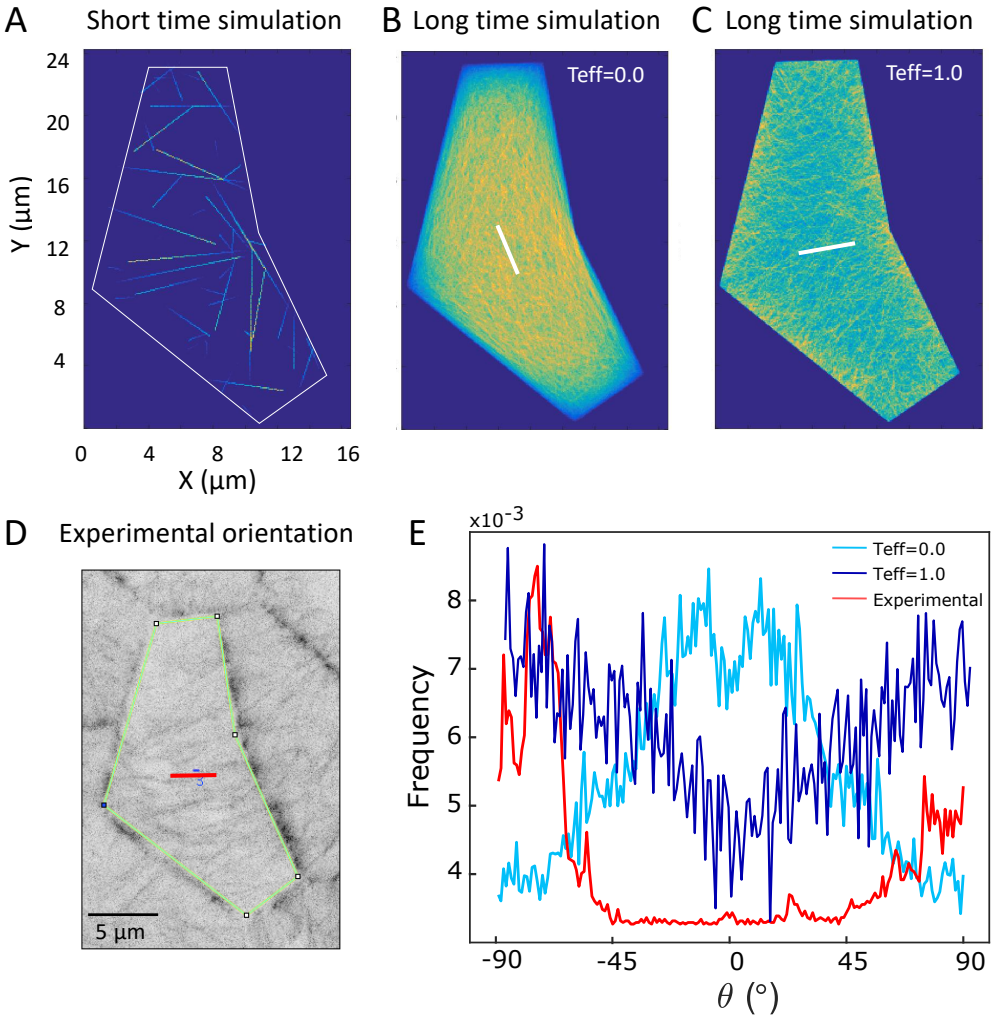

Figure 25: Density profile and distribution of angular orientations extracted from the two-state dynamic instability model.

The colormap in density profiles (**A-C**) is the frequency of microtubules from high density (yellow) to low density (blue). **A**, Simulation of 20 MTs after a few iterations of the algorithm present in the main text. **B**, Density profile extracted from simulation of 80 MTs inducing catastrophe as a boundary condition ($\tau_{\text{eff}} = 0.0$). **C**, Density profile extracted from simulation of 80 MTs and inducing pause time as boundary condition ($\tau_{\text{eff}} = 1.0$). **D**, Microtubule orientation obtained from the Fiji plugin, FibrilTool. The global orientation was measured in a cell image of the GFP-tub *Marchantia* line. The global orientation in this cell was $87.02°$. **E**, Distribution of angular orientation from the condition represented in B (light blue), C (blue) and experimental orientation obtained from image in D (red) .The results showed that, inducing a pause time ($\tau_{\text{eff}} = 1.0$) is possible to reproduce the distribution obtained from experimental data.

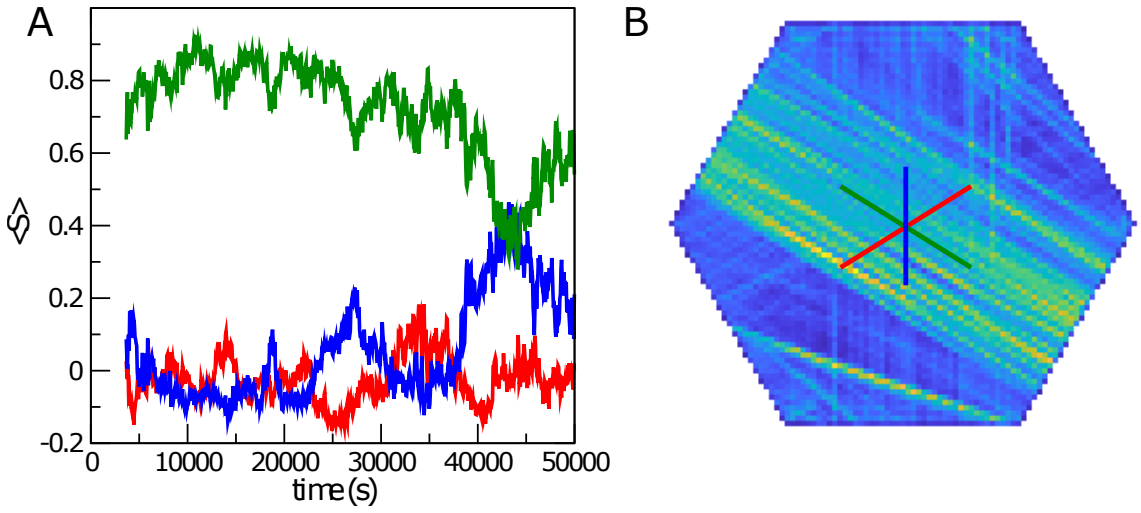

Figure 26: Microtubules nucleating in an orthogonal direction to the edge can reproduce the preprophase band formation.

Total number of MT $N = 100$. Pause time at the edge $\tau = 1$. $p = 0.75$ (75% of MT nucleated at the edge). **A**, Value of S calculated along the three alternatives division planes; $30°$, $90°$ and $150°$ indicated with the color green, blue and red, respectively. **B**, Density profile of the MT nucleated at the edge.

Using a realistic cell shape, we simulated 100 MTs with different probability to be nucleated in the center or along the edge by different p values $(0.1, 0.2, 0.4)$ (Figure 27C). Also, considering $p = 0.5$ we simulated the dynamic using 80, 90 and 100 MTs (Figure 27D). The vertical or horizontal direction was considered to measure the alignment by S value during the simulation. Also, we calculated the S value from our experimental data, which was compared with the simulation. The results showed that the simulation could reproduce the experimental data when 50% of MTs are nucleated along the edge ($p = 0.5$) (Figure 27C). Also, simulating the dynamic of 100 MTs fit better with the experimental results (Figure 27D). Under dynamic conditions described, we were not able to observe the formation of the PPB in that shape (Figure 27B). However, we could recreate the set of MT orientations observed during the

PPB formation, which is closer to the array arrangement observed in time 0 (Figure 27A,B).

The orthogonal nucleation of MTs along the edge influences the MT array organization. Based on our observations, this orientation came from the anticlinal face, therefore, to consider the anticlinal faces in the simulation could provide new features of the MT organization. We simulated a rectangular prism, where are represented the anticlinal and periclinal faces (Figure 28A). For the simulation, we considered MTs randomly nucleated and oriented within the cell surface. Also, we included two different conditions; In the first one, the MTs reaching the edge pause and have an 80% probability of passing to the next side ($p_t = 0.8$). In the second one, the MTs reaching the edge pause, and do not cross to the other face (control condition). In both conditions, we could reproduce an orthogonal distribution of MTs on the border of the periclinal face. Considering the first condition, we could reproduce the orthogonal MT distribution along the edges observed *in vivo* (Figure 28B). Also, we could reproduce a narrowing of the MTs in the middle, which is similar to a PPB structure (Figure 28C).

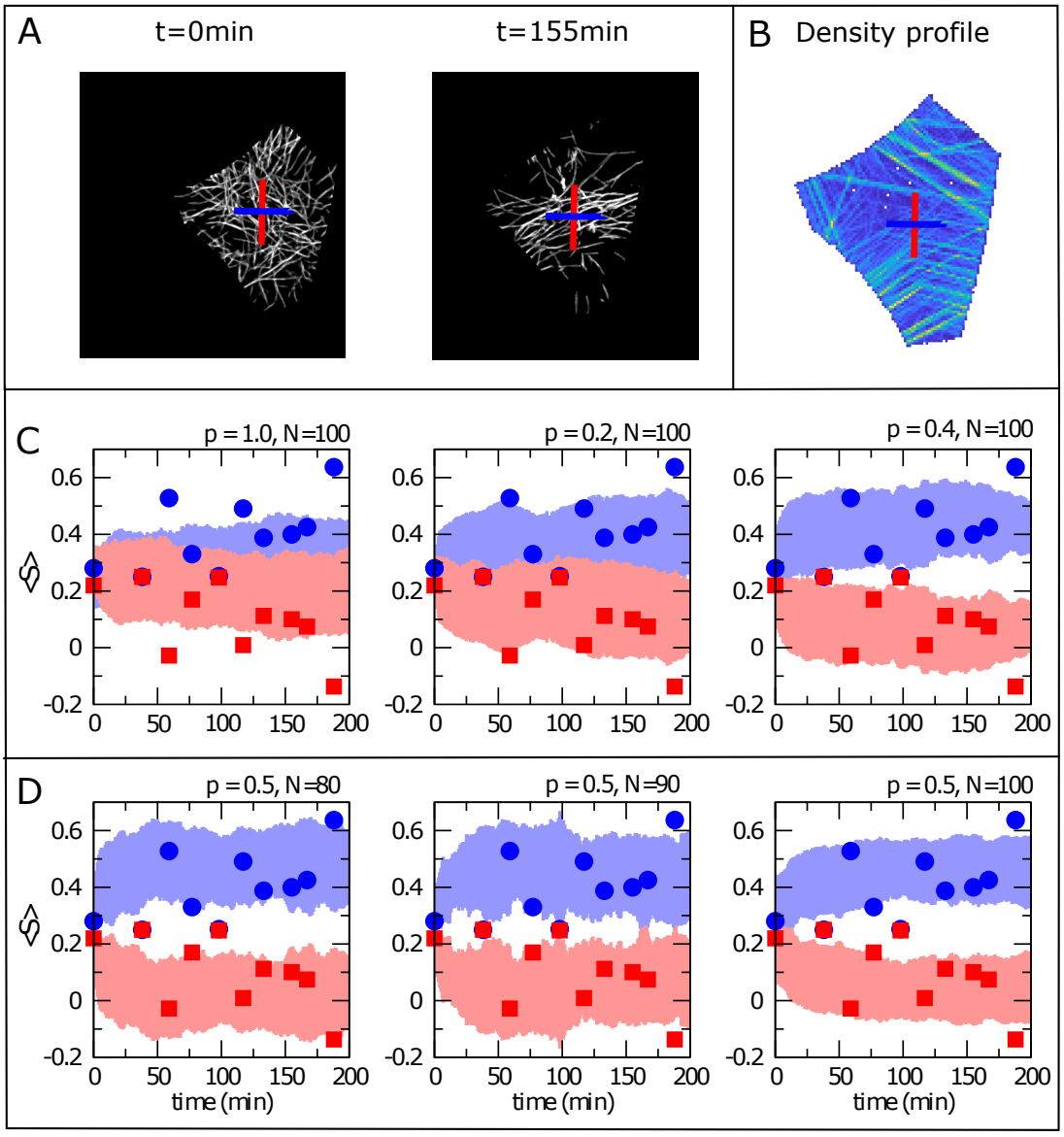

Figure 27: The microtubule alignment obtained during the simulation fit with the experimental distribution observed during the preprophase band formation.

A, Start and end time point from the time-lapse registered during PPB formation. **B**, Density profile obtained after 200 min of simulation. **C-D**, Alignment along the vertical and horizontal direction as a function of time. The colored area is averaged from a large number of independent simulations, the symbols, red squares and blue circles, are S value for the experimental observations. p is the fraction of MT nucleated randomly in the center of the cell, N is the total number of MTs.

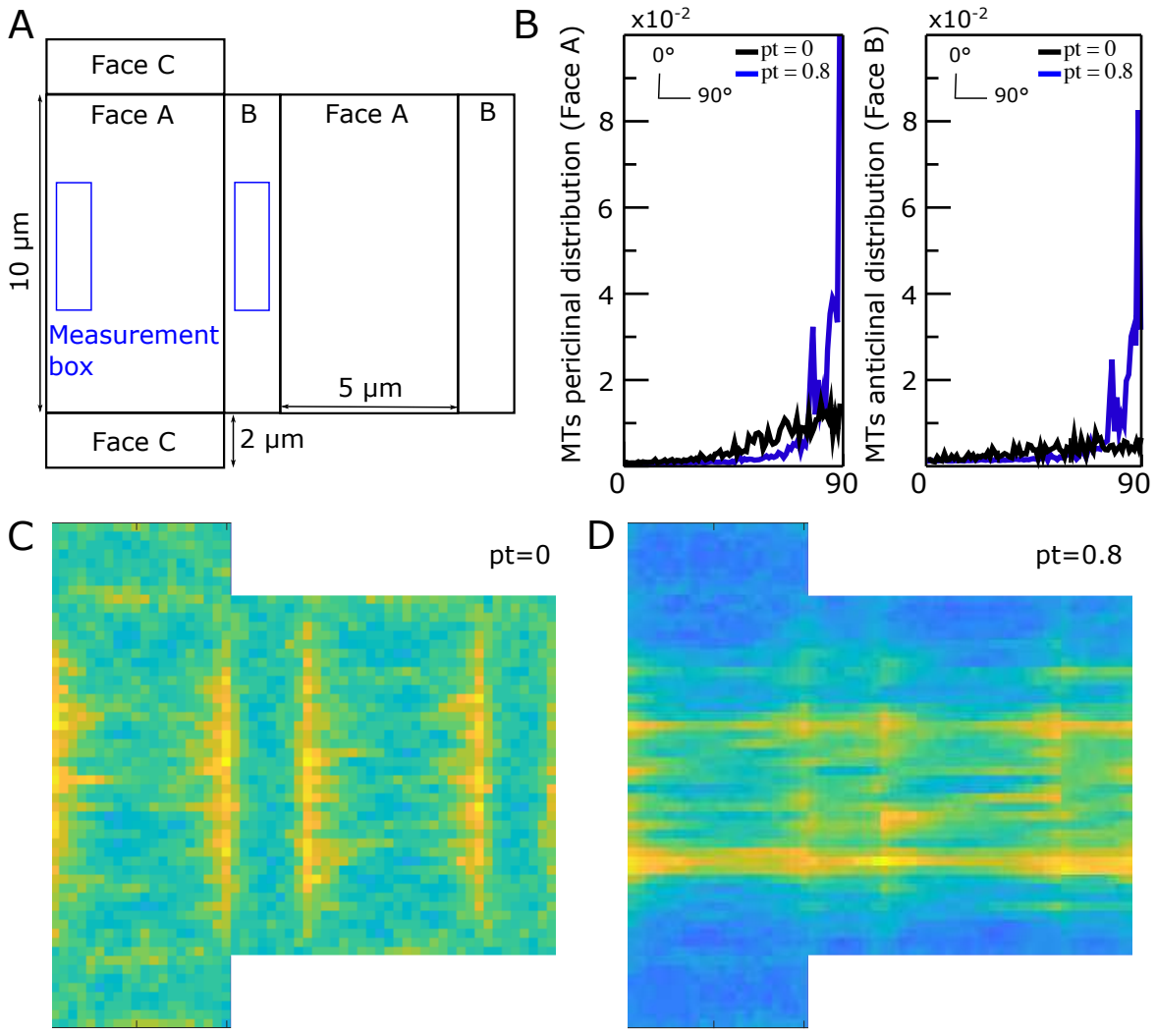

Figure 28: 3D Simulation can reproduce the orthogonal orientation and the preprophase band.

A, Flattened rectangular prism used in the simulation. Anticlinal faces correspond to Faces, B and C. Periclinal faces correspond to the faces A. The MTs orientation of specific areas on the periclinal and anticlinal was measured. The measurement areas are indicated with the blue boxes. When a MT reaches an edge, it pauses with a duration of $l_0/v_0 = 430\,\mathrm{s}$. After the pause, the MT can either continue growing on the other face with a probability p_t, or undergoes a catastrophe and shrink with a probability $1 - p_\mathrm{t}$. The number of MT simulated on the surface is 100. MTs are nucleated randomly within one of the six faces. **B**, Angle distribution on the face A and B using two border conditions; $p_\mathrm{t} = 0$ and $p_\mathrm{t} = 0.8$. **C**, Density profile for the border condition $p_\mathrm{t} = 0$. **D**, Density profile for the border condition $p_\mathrm{t} = 0.8$.

6.3 Deviation from the cell division rule in the trm678 mutant of *Arabidopsis thaliana*.

We worked on this objective using the triple mutant trm678 line of Arabidopsis, co-expressed with KA1, a domain that interact with the membrane by anionic phospholipids. This line was provided by the team of Dr. David Bouchez of INRA Centre de Versailles-Grignon, France, collaborator in the Human Frontier Science Program (HFSP) project. The triple mutant trm678 shows a disruption in PPB formation, and as a consequence, the division rule could be affected. Thus, we followed the formation of new division planes to test the geometrical rule of cell division in this mutant line. We dissect the meristem, and it was mounted to observe under confocal microscope. We took images of the meristem after the dissection ($t = 0$ h) and after 16 h. We selected the cells recently divided to extract the cell shape and predict the alternatives division planes. The cell division observed was compared with each alternatives division planes to classify in mode 1, mode 2, mode 3, mode 4 and others. The wild type showed that 71.21%, 10.9%, 4.6%, 3.2% and 10.1% of the cells are dividing along the mode 1, mode 2, mode 3, mode 4 and others, respectively. The wild type data was supplemented by the data published by Louveaux et al., 2016. Whereas, the mutant line showed that 42.11%, 10.53%, 18.42%, 5.26% and 23.68% of the cells are diving along the mode 1, mode 2, mode 3, mode 4 and others, respectively. Comparing the histograms of the mutant and the wild type lines, the results showed abnormalities in the cell division of the mutant line. For instance, a 23.68% of the cells in the mutant line form a division plane in a position that does not

correspond to any predicted division plane, compared with 10.1% of the wild type (Figure 29).

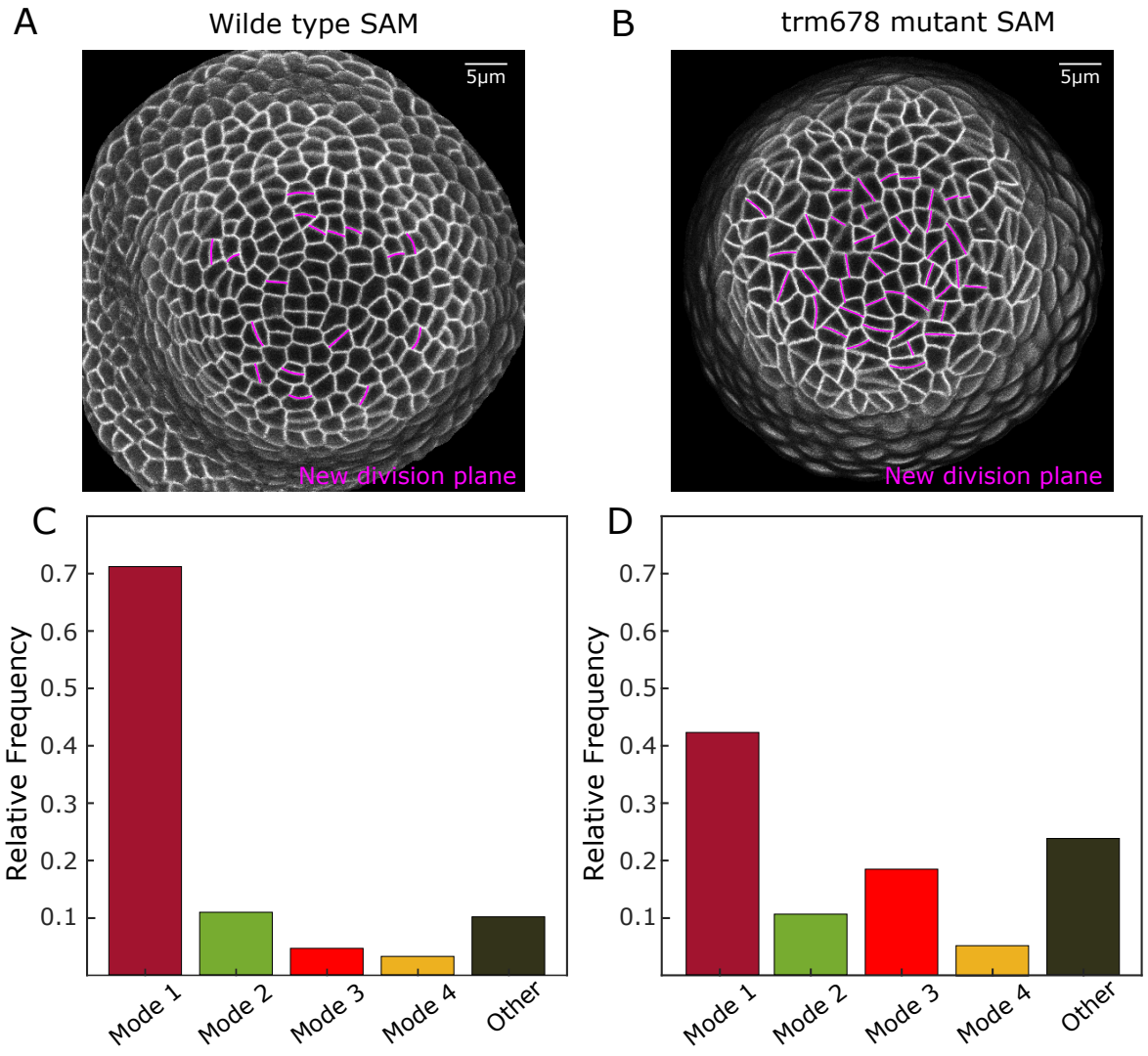

Figure 29: trm678 mutant line of *Arabidopsis thaliana* do not follow the geometrical rule.

Shoot apical meristem of wild type and trm678 mutant was observed in order to follow new cell divisions and test the geometrical rule for cell division. **A-B**, After $16\,h$, new division planes were observed and indicated in the meristem using magenta curves. **C**, Frequencies of different division modes for the cells of wild type line. Overall, 71.21%, 10.9%, 4.6%, 3.2% and 10.1% of the cells divide along the shortest plane, second shortest, third shortest, fourth shortest and others, respectively. $N = 653$. Our data was complemented by the published data from Louveaux et al. 2016. **D**, Frequencies of different division modes for the cells of trm678 mutant line. Overall, 42.11%, 10.53%, 18.42%, 5.26% and 23.68% of the cells divide along the shortest plane, second shortest, third shortest, fourth shortest and others, respectively. $N = 38$.

7. DISCUSSION

Division rules for plant cells were first proposed in the nineteenth century by Errera and Sachs, and later reformulated as a probabilistic rule by Besson and Dumais (Besson and Dumais, 2011; Errera, 1886; Sachs, 1878). It has been shown that the position of the division plane is determined by the site of the PPB, a structure arising from the self-organization of cortical MTs (Ôta, 1961; Van Damme and Geelen, 2008). Numerous studies have addressed the key dynamic properties contributing to the self-organization of MT structures (Dixit and Cyr, 2004; Palevitz and Hepler, 1974; Pickett-Heaps, 1974; Subramanian and Kapoor, 2012). However, it is still unclear how those dynamic properties influence PPB formation. Our results show that the standard dynamic properties of MTs and the interaction of MTs with the cell edges are sufficient to form the PPB in least-area configurations. In the following pages, we discuss the principal findings of this thesis and how these help explain the selection of a division plane in plant cells.

7.1 *Marchantia polymorpha* cells follow the geometrical division rule.

According to Errera, plant cells divide along planes whose geometries represent local area minima enclosing a fixed cellular volume to create two daughter cells of nearly equal size (Besson and Dumais, 2011; Errera, 1886; Sachs, 1878). This division rule was tested in our model system, *Marchantia*. We found that the great majority of cells select the shortest division plane (78.8%), while fewer cells select the second, third and fourth shortest division planes (Figure 12). This probability distribution follows

closely the trend observed in other species, such as *Arabidopsis thaliana*, *Microsorum punctatum* and *Zinnia elegans* (Besson and Dumais, 2011; Louveaux et al., 2016). In addition, the control parameter for the probability distribution measured in *Marchantia* ($\beta = 19.4$) falls within the range previously observed, thus establishing a near universal probability distribution for species spanning the entire tree of land plants who, together, represent more than 500 million years of evolution (Lang et al., 2010; Sanderson et al., 2004) (Figure 13).

The correlation of the division plane with cell shape was observed also in animal cells. Hertwig captured this tendency in his long axis rule: "The two poles of the division figure come to lie in the direction of the greatest protoplasmic mass" (Hertwig, 1884). However, Minc and colleagues found that this rule does not apply for some specific cell shapes. They developed a computational model that fully predict the preferred division plane and the probability that an axis will be chosen for a given cell shape. The model developed by Minc et al. proposed that shape sensing could be explained by a mechanism based upon microtubule length-dependent forces (Minc et al., 2011). In addition to this model, Campinho and coworkers found in the enveloping cell layer (EVL) of zebrafish that the division plane orientation requires myosin II activity to align the mitotic spindle with the cell elongation axis (Campinho et al., 2013). Thus, in animal cells, the mechanism behind the nuclear and mitotic spindle positioning is a process that involves motor proteins exerting forces from MTs and/or the actin cytoskeleton (Grill et al., 2005; Kunda and Baum, 2009; Minc et al., 2011; Reinsch and Gönczy, 1998; Wühr et al., 2009).

For plant cells, Besson and Dumais offered an analogous mechanism to explain

the positioning of the division plane, where the tensional forces would constrain cytoskeletal strands to span the shortest distance between the nucleus and the cell surface (Besson and Dumais, 2011). These findings suggest a common, microtubule-dependent, mechanism that allows the cell to sense cell shape and to guide the division plane positioning.

7.2 Global analysis of microtubule orientation in early interphase.

To study how MT orientation can track cell geometry, we acquired images of interphase MTs. We found that 50% of the cells showed MTs following the shortest division plane (Figure 16). This observation suggests that MTs could follow the cell division rule even before the formation of the PPB. However, almost 80% of *Marchantia* cells select the shortest division plane in accord with our observations (Figure 12). This difference can probably be explained by the evolving dynamics of MT arrays during interphase.

The co-alignment of cortical MTs in interphase is characteristic of plant cells. Interphase MT arrays are involved in guiding cellulose microfibril deposition in an orientation that is commonly perpendicular to the growth axis (Dixit and Cyr, 2004). However, time-lapse observation of MT arrays in interphase has revealed consistent spatial and temporal re-organization of these structures (Granger and Cyr, 2001; Lindeboom et al., 2013; Sugimoto et al., 2000; Vineyard et al., 2013). These studies provide interesting data suggesting that microtubule self-organization in an acentrosomal system evolves as the cell progresses between the different cell cycle states (Elliott and Shaw, 2018). This progressive evolution could explain

the difference we found between the orientation of the cell division planes and the orientation of interphase MTs.

Future work should include long-term observations of MT arrays during interphase to quantify their dynamics and generate a more precise relation between microtubule orientation and the selection of the division plane. Moreover, given the importance of the cell cycle timing in the organization of MTs, future experiments should use transgenic lines with cell cycle markers to get a more precise timing of the maturation of MT arrays.

7.3 Local analysis of microtubule orientation along the predicted division planes in late interphase.

The PPB is formed during late interphase, starting first with the formation of polar organizers, which we used as a marker to choose the cells to be observed (Buschmann et al., 2016). We analyzed the local MT distribution along the alternative division planes at the beginning of PPB formation. The results showed that MTs have a predominant alignment along mode 1 and 3, which is different from the predominant mode 1 alignment of MTs observed in early interphase. This discrepency, in addition to a β value of 0.5, shows that the orientation of cortical MTs at this stage does not follow Errera's Rule (Figure 18). Therefore, it was not possible to predict the future division plane based on the local MT alignment.

Although, these results are not in agreement to our previous finding, there are many reasonably explanations for this difference. First, we detected in the vector

field a few false positive signals, that could increase the noise of the quantification, specially because of the small area analyzed. Second, to compare this result with the MT orientations observed in early interphase, it is necessary to quantify the global orientation on this dataset. Third, the cell cycle time when the alignment was quantified is in late interphase, when mitotic signals are present and, therefore, the MT arrangement could be altered compared to the MT organization in early interphase (Figure 16). Fourth, based on the geometrical cell division rule, MT organization responds to a stochastic process. This can result in different MT arrangements for the same cell shape. In this context, the size of the dataset influences the subsets of MT organization that can be observed for a given cell shape. We analyzed 48 cells with different shapes, which is still a small number to observe reliably the alternative MT arrangements.

In the future, it would be interesting to quantify the MT local alignment along more than four alternative division planes. Thus, we could test if the MT alignment is random among the shortest alternative division planes predicted or among any possible alternative division plane. If the highest probability corresponds to the fourth shortest division plane predicted, this could suggest that the MTs do not have a totally random distribution at the beginning of the PPB formation. Thus, the distribution of the array would show a reduced number of options that could progress at the end.

Considering the extensive evidence supporting the role of MTs in selecting the division plane in both animal and plant cells, it becomes necessary to develop a model based on the local MT dynamics, independent of the geometrical division rule. This could provide a more robust model to predict the division plane.

7.4 Analysis of microtubule orientation near to the cell edges in late interphase.

To study the transition between the MT pattern in interphase and the PPB, we performed local analyses of MT orientation during the transition process. We observed that MTs at the periphery of the periclinal face were consistently orthogonal to the closest cell edge (Figure 20). The cells observed in *Marchantia* have variable shapes, including symmetrical and highly asymmetrical cell geometries. Thus, our results revealed that the orthogonality of MTs with the nearest cell edge is conserved for any cell geometry. Interestingly, this finding is predicted by the cell division rule, which states that new division planes reach the older wall at 90 degrees. The orthogonal MT distribution is also observed in hypocotyl and root cells in *Arabidopsis thaliana* (Thoms et al., 2018; Vineyard et al., 2013); however, these cells are elongated rectangular cells where the orthogonal orientation of MTs also coincide to the geometrical axis of the cell.

Using 3D visualization, we observed that 63% of the orthogonal MTs found along the edges of the periclinal face also extend to the anticlinal face (Figure 22A-B). Moreover, a more detailed analysis of our movies reveals that 68% of MTs grow from the anticlinal face towards the periclinal face (Figure 23). Vineyard and coworkers found that the transverse array organization in hypocotyl cells is maintained by new transverse MTs emerging from the anticlinal faces that compete with the longitudinal MTs in the periclinal face, which are directly targeted for destruction (Vineyard et al., 2013). This finding is compatible with our observations, suggesting that a competition

among subsets of MTs in the periclinal face can be an important component of the mechanism for MT organization. This competition would favor MTs in a specific direction over other directions, which ultimately could cause a narrowing of the MT array in the middle of the cell, similar to a PPB.

7.5 Biophysical model of microtubule dynamics and cell border interactions during PPB formation.

The biophysical model developed reveals the importance of MT interactions with the cell edges as a mechanism to achieve short-axis alignment of MT arrays. Using a realistic cell shape, our simulations showed that with a pause time τ_{eff} of 0 (catastrophe-inducing edges), MTs are preferentially aligned with the longest axis of the cell. In contrast, for a pause state τ_{eff} of 1.0, the MT alignment is along the short axis of the cell, as observed experimentally (Figure 25). In a biological context, the CLASP protein, present in both animal and plant cells, could play a role similar to our pause time by stabilizing MTs at the cell edges and helping them to bend and cross to the other cell face (Thoms et al., 2018).

Moreover, co-expression of GFP-CLASP1 and RFPTubulin6 show the co-localization of these signals in transfacial microtubules on sharp cell edges (Ambrose et al., 2011). In addition, the sharp edges in the clasp-1 mutant induced depolymerization and catastrophe of MTs, with a consequent decrease in transfacial MTs (Ambrose et al., 2011). The sharp edges could be a local physical barrier because MTs require extra energy to bend the tubulin lattice to pass from one cell face to another. Therefore, CLASP would act by buffering that effect, allowing the stabilization of MTs in that

zone and enabling MTs to grow perpendicular to sharp cell edges (Ambrose et al., 2011; de Keijzer et al., 2014). In this context, our results supported fully the evidence that MTs orientation depends on cell geometry.

The experimental results showed orthogonal MT orientation along the cell edges (Figure 20). We implemented this feature in our model, nucleating MTs at the cell edges with a uniform probability. At steady-state, we observed the formation of a band of MTs in the main direction corresponding to one of the alternative division planes. This finding confirms that the competition among families of MTs can cause the formation of a PPB-like structure (Figure 26).

Previous models developed to understand transverse array patterning indicated that MT organization is driven by preferential loss of longitudinally oriented microtubules at apical and basal ends of the cells (Allard et al., 2010; Ambrose et al., 2011; Baulin et al., 2007; Ehrhardt and Shaw, 2006; Eren et al., 2010). These models suggest that if microtubules at the apical and basal ends of the cell are prevented from entering the outer periclinal array or are selectively destroyed through catastrophes at cell edges, then the remaining MTs will naturally form a transversely align array (Ambrose et al., 2011). The degree of microtubule co-alignment for the remaining microtubules is hypothesized to improve through the action of angle-dependent bundling (Allard et al., 2010; Eren et al., 2010).

The models developed to date suggest a mechanism to explain the transverse array pattern, including differential border conditions. We developed a model that includes general rules for the borders in accordance with our experimental observations, which can explain the cortical MT orientation and its self-organization to form the PPB.

Further analysis leads us to conclude that MT orientation along the cell edges can be explained if we considered the anticlinal faces of the cell. Here, without imposing orthogonal MT orientation to the edge, we could reproduce the orthogonal orientation observed experimentally at the border of the periclinal face and also form a PPB-like structure on the shortest division plane (Figure 28).

Finally, our results suggest that cell shape and MT dynamics are sufficient to form the PPB. However, we still have to extend the simulations to realistic 3D shapes and quantify the accuracy of our model to predict the division plane orientation based on the mechanism proposed in this thesis. Moreover, it is still important to contrast the mechanism postulated by the model with the cortical MT array dynamics observed during the PPB formation. In this context, studies of the dynamics of cortical MT arrays in trm678 mutants of *Marchantia* could provide us with critical data about the key element behind this specific MT self-organization process.

To sum up, we proposed a model where the dynamic instability of MTs, MT-MT interactions, and MT-cell edge interactions contribute to the formation of MT arrays along the shortest axis of cells irrespective of their geometry. Moreover, bundling of MTs within the array and depletion of MTs at the cell corners can explain the formation of PPB-like structures (Figure 30).

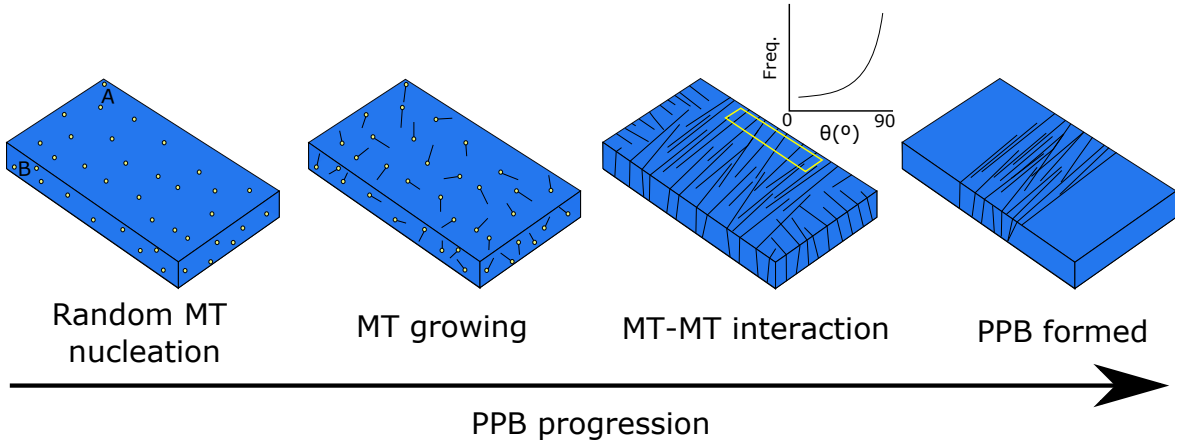

Figure 30: Representation of the biophysical model for the PPB formation.
First rectangular prism (left), yellow dots represent the initial random nucleation around the periclinal face (A) and anticlinal face (B). Second rectangular prism, black straight line represents the random growing direction after the simulation start. Third rectangular prism, straight lines around the faces represent the MT array when the orthogonal direction from the edge (yellow box) starts to be established. Fourth rectangular prism represents the condensed array in the center (PPB).

7.6 Biomedical outlook.

This thesis highlights a possible mechanism for the establishment of the PPB in plant cells. We determined that the dynamic properties of MTs and the interaction with the cell edges are key for the self-organization of MT arrays and the formation of the PPB. Thus, our findings clarify the mechanism behind the positioning of the division plane in plant cells. Moreover, given the common features between animal and plant cells, it is also possible to revisit our findings in the context of biomedical research.

The establishment of a cell division plane has been of interest to both plant and animal biologists. Historically, this research has led to homologous cell division rules: Errera's Rule for plant cells and Hertwig's Rules for animal cells, suggesting that the underlying mechanisms may be fundamentally equivalent. Moreover, MTs are

highly conserved subcellular structures across the eukaryotic kingdoms (Wasteneys, 2002). MT organizations are different between cell types, however, plant cells share a non-centrosomal organization with specialized cells in animals, such as epithelial, neurons and muscle cells (Bartolini and Gundersen, 2006).

In animals, the mis-orientation of cell division can cause defects in tissue architecture, cell fate mis-specification and cancer. Specifically, spindle mis-orientation has been attributed to changes in cell shape and loss of cortical contact of astral MTs. Such defects were observed in colon cancer caused by mutation of the APC tumor suppressor, which participates in the stabilization of MTs (Pease and Tirnauer, 2011). Another disease associated with a defective cell division orientation is the autosomal recessive primary microcephaly. This disease results in an increase of asymmetric cell divisions and a loss of neuroepithelial cells abutting the ventricular zone (Fish et al., 2006). Consequently, microcephalic brains do not contain the same amount of cells as their wild-type counterparts, manifested in the small brain phenotype. Mis-orientation of cell division can lead, moreover, to cell fate problems during animal tissue development. For instance, an increasing number of vascular development disorders have been reported to result from spindle orientation defects (Wu et al., 2020). In this context, electrical stimulation has emerged as a novel approach to induce reorientation of the spindle along the long axis of endothelial cells, and perpendicular to the electric field vector (Cunha et al., 2019; Zhao et al., 2004). Electric stimulation has been widely used to induce neurogenic and cardiomyogenic regeneration through regulating endothelial cell migration to wound site and affecting endothelial cell division orientation (Jeong et al., 2017; Ragnarsson, 2008; Zhang

et al., 2011; Zhao et al., 2004). A better understanding of the biological effects of electrical stimulation might lead to new therapies of tissue regeneration to treat diseases or conditions in which division planes are mis-oriented (Cunha et al., 2019).

Finally, in contrast to animal cells, plant cells are surrounded by rigid walls and, as a result, are immobile. Therefore, the orientation of the cell division plane is critical to determine tissue organization and growth in plants (Smolarkiewicz and Dhonukshe, 2013). The fixed cell shape forced by the wall of plant cells is interesting because it offers a natural model to understand the relationship between cell shape and the establishment of the division plane; whereas the less definite cell shapes of animals has forces investigators to work in vitro, using micromanipulations to control cell shape (Minc et al., 2011).

8. CONCLUSIONS

This thesis has revealed the most important processes behind the self-organization of MTs to position and establish the PPB. Our most important findings lead us to the following statements:

- The bryophyte *Marchantia polymorpha* follows the cell division rule shared by a broad range of plant taxa including angiosperms, ferns and coleochaetales.
- Interphase MTs are able to sense cell shape, orienting themselves along the shortest axis of the cell.
- Based on our biophysical model, the dynamic instability of MTs, MT-MT interactions and MT-cell edge interactions are sufficient to explain the formation of the PPB.

Therefore, the hypothesis proposed in this thesis was confirmed.

9. PUBLICATIONS

Manuscript in preparations:

Title: Mechanism Based on Microtubules Self-organization to Predict Cell Division Orientation.

Authors: Paula Llanos, Simon Gravelle, Olivier Hamant, Jim Haseloff, Henrik Buschmann, Steffen Hartel, Mauricio Cerda, Jacques Dumais.

Title: Microscopic Mechanism for Errera's Rule: Short Axis Selection by Self-organizing Microtubules.

Authors: Simon Gravelle, Paula Llanos, Jacques Dumais.

10. ACKNOWLEDGEMENTS

10.1 Funding.

Ph.D. National Funding, CONICYT, Chile.

FONDECYT regular 2018 Nº 1180906, Universidad Adolfo Ibáñez, Chile.

Human Frontier Science Program RG2018, ENS-Lyon, France.

10.2 Sponsoring Laboratories.

Laboratory of Bioengineering, Universidad Adolfo Ibáñez, Chile. Prof. Jacques Dumais.

Laboratory for Scientific Image Analysis, Universidad de Chile, Chile. Prof Steffen Härtel and Prof. Mauricio Cerda.

Laboratory Mechanotransduction in Development, École Normale Supérieure of Lyon, France. Prof. Olivier Hamant.

Laboratory of Synthetic Biology, University of Cambridge, UK. Prof. Jim Haseloff.

Laboratory of Botany, University of Osnabrück, Germany. Prof. Henrik Buschmann.

Imaging and Microscopy Core Facility, École Normale Supérieure of Lyon, France.

11. REFERENCES

Akhmanova, A. and Steinmetz, M. O. (2008). Tracking the ends: A dynamic protein network controls the fate of microtubule tips. *Nat. Rev. Mol. Cell Biol.*, 9:309–322.

Akhmanova, A. and Steinmetz, M. O. (2010). Microtubule +TIPs at a glance. *J. Cell Sci.*, 123:3415–3419.

Al-Bassam, J., Kim, H., Brouhard, G., van Oijen, A., Harrison, S. C., and Chang, F. (2010). CLASP promotes microtubule rescue by recruiting tubulin dimers to the microtubule. *Dev. Cell*, 19(2):245–258.

Allard, J. F., Wasteneys, G. O., and Cytrynbaum, E. N. (2010). Mechanisms of self-organization of cortical microtubules in plants revealed by computational simulations. *Mol. Biol. Cell*, 21(2):278–86.

Ambrose, C., Allard, J. F., Cytrynbaum, E. N., and Wasteneys, G. O. (2011). A CLASP-modulated cell edge barrier mechanism drives cell-wide cortical microtubule organization in Arabidopsis. *Nat. Commun.*, 2(1):430–442.

Ambrose, C. and Wasteneys, G. O. (2012). Nanoscale and geometric influences on the microtubule cytoskeleton in plants: Thinking inside and outside the box. *Protoplasma*, 249(1):69–76.

Bartolini, F. and Gundersen, G. G. (2006). Generation of noncentrosomal microtubule arrays. *J. Cell Sci.*, 119(20):4155–63.

Baulin, V. A., Marques, C. M., and Thalmann, F. (2007). Collision induced spatial organization of microtubules. *Biophys. Chem.*, 128(2-3):231–44.

Besson, S. and Dumais, J. (2011). Universal rule for the symmetric division of plant cells. *Proc. Natl. Acad. Sci.*, 108(15):6294–6299.

Bhowmick, N. A., Neilson, E. G., and Moses, H. L. (2004). Stromal fibroblasts in cancer initiation and progression. *Nature*, 432(7015):332–337.

Bichet, A., Desnos, T., Turner, S., Grandjean, O., and Höfte, H. (2001). BOTERO1 is required for normal orientation of cortical microtubules and anisotropic cell expansion in Arabidopsis. *Plant J.*, 25(2):137–48.

Boudaoud, A., Burian, A., Borowska-Wykręt, D., Uyttewaal, M., Wrzalik, R., Kwiatkowska, D., and Hamant, O. (2014). FibrilTool, an ImageJ plug-in to quantify fibrillar structures in raw microscopy images. *Nat. Protoc.*, 9(2):457–463.

Bouquin, T., Mattsson, O., Naested, H., Foster, R., and Mundy, J. (2003). The Arabidopsis lue1 mutant defines a katanin p60 ortholog involved in hormonal control of microtubule orientation during cell growth. *J. Cell Sci.*, 116(5):791–801.

Bratman, S. V. and Chang, F. (2007). Stabilization of Overlapping Microtubules by Fission Yeast CLASP. *Dev. Cell*, 13(6):812–827.

Burk, D. H., Liu, B., Zhong, R., Morrison, W. H., and Ye, Z. H. (2001). A katanin-like protein regulates normal cell wall biosynthesis and cell elongation. *Plant Cell*, 13(4):807–27.

Buschmann, H., Holtmannspötter, M., Borchers, A., O'Donoghue, M. T., and Zachgo, S. (2016). Microtubule dynamics of the centrosome-like polar organizers from the basal land plant Marchantia polymorpha. *New Phytol.*, 209(3):999–1013.

Campinho, P., Behrndt, M., Ranft, J., Risler, T., Minc, N., and Heisenberg, C. P. (2013). Tension-oriented cell divisions limit anisotropic tissue tension in epithelial spreading during zebrafish epiboly. *Nat. Cell Biol.*, 15(12):1405–1414.

Chakrabortty, B., Willemsen, V., de Zeeuw, T., Liao, C. Y., Weijers, D., Mulder, B., and Scheres, B. (2018). A Plausible Microtubule-Based Mechanism for Cell Division Orientation in Plant Embryogenesis. *Curr. Biol.*, 28(19):3031–3043.e2.

Cleary, A. L., Gunning, B. E., Wasteneys, G. O., and Hepler, P. K. (1992). Microtubule and F-actin dynamics at the division site in living Tradescantia stamen hair cells. *J. Cell Sci.*, 103(4):977–988.

Coquelle, F. M., Vitre, B., and Arnal, I. (2009). Structural basis of EB1 effects on microtubule dynamics. *Biochem. Soc. Trans.*, 37(5):997–1001.

Costa, S. (2017). Are division plane determination and cell-cycle progression coordinated? *New Phytol.*, 213(1):16–21.

Cunha, F., Rajnicek, A. M., and Mccaig, C. D. (2019). Electrical Stimulation Directs Migration, Enhances and Orients Cell Division and Upregulates the Chemokine Receptors CXCR4 and CXCR2 in Endothelial Cells. *J. Vasc. Res.*, 56(1):39–53.

de Keijzer, J., Mulder, B. M., and Janson, M. E. (2014). Microtubule networks for plant cell division. *Syst. Synth. Biol.*, 8(3):187–194.

Deinum, E. E., Tindemans, S. H., Lindeboom, J. J., and Mulder, B. M. (2017). How selective severing by katanin promotes order in the plant cortical microtubule array. *Proc. Natl. Acad. Sci.*, 114(27):6942–6947.

Dhonukshe, P. and Gadella, T. W. J. (2003). Alteration of microtubule dynamic instability during preprophase band formation revealed by yellow fluorescent protein-CLIP170 microtubule plus-end labeling. *Plant Cell*, 15(3):597–611.

Dixit, R. and Cyr, R. (2004). Encounters between dynamic cortical microtubules promote ordering of the cortical array through angle-dependent modifications of microtubule behavior. *Plant Cell*, 16(12):3274–84.

Dixit, R. and Cyr, R. J. (2002). Spatio-temporal relationship between nuclear-envelope breakdown and preprophase band disappearance in cultured tobacco cells. *Protoplasma*, 219(1-2):116–21.

Drakakaki, G. (2015). Polysaccharide deposition during cytokinesis: Challenges and future perspectives. *Plant Sci.*, 236:177–184.

Drechsel, D. N., Hyman, A. A., Cobb, M. H., and Kirschner, M. W. (1992). Modulation of the dynamic instability of tubulin assembly by the microtubule-associated protein tau. *Mol. Biol. Cell*, 3(10):1141–54.

Ehrhardt, D. W. and Shaw, S. L. (2006). Microtubule Dynamics and Organization in the Plant Cortical Array. *Annu. Rev. Plant Biol.*, 57(1):859–875.

Elliott, A. and Shaw, S. L. (2018). Update: Plant cortical microtubule arrays. *Plant Physiol.*, 176(1):94–105.

Eren, E. C., Dixit, R., and Gautam, N. (2010). A Three-Dimensional Computer Simulation Model Reveals the Mechanisms for Self-Organization of Plant Cortical Microtubules into Oblique Arrays. *Mol. Biol. Cell*, 21(15):2674–2684.

Eren, E. C., Gautam, N., and Dixit, R. (2012). Computer simulation and mathematical models of the noncentrosomal plant cortical microtubule cytoskeleton. *Cytoskeleton*, 69(3):144–154.

Errera, L. (1886). Sur une condition fondamentale d'équilibre des cellules vivantes. *C R Hebd Seances Acad Sci*, 103:822–824.

Fish, J. L., Kosodo, Y., Enard, W., Pääbo, S., and Huttner, W. B. (2006). Aspm specifically maintains symmetric proliferative divisions of neuroepithelial cells. *Proc. Natl. Acad. Sci.*, 103(27):10438–10443.

Galatis, B., Apostolakos, P., and Katsaros, C. (1984). Experimental studies on the function of the cortical cytoplasmic zone of the preprophase microtubule band. *Protoplasma*, 122(1-2):11–26.

Galjart, N. (2010). Plus-end-tracking proteins and their interactions at microtubule ends. *Curr. Biol.*, 20(12):R528–37.

Gardner, M. K., Zanic, M., and Howard, J. (2013). Microtubule catastrophe and rescue. *Curr. Opin. Cell Biol.*, 25(1):14–22.

Granger, C. and Cyr, R. (2001). Use of abnormal preprophase bands to decipher division plane determination. *J. Cell Sci.*, 114(3):599–607.

Grill, S. W., Gönczy, P., Stelzer, E. H., and Hyman, A. A. (2001). Polarity controls forces governing asymmetric spindle positioning in the caenorhabditis elegans embryo. *Nature*, 409(6820):630–633.

Grill, S. W., Howard, J., Schäffer, E., Stelzer, E. H., and Hyman, A. A. (2003). The distribution of active force generators controls mitotic spindle position. *Science*, 301(5632):518–521.

Grill, S. W. and Hyman, A. A. (2005). Spindle Positioning by Cortical Pulling Forces. *Dev. Cell*, 8(4):461–465.

Grill, S. W., Kruse, K., and Jülicher, F. (2005). Theory of mitotic spindle oscillations. *Phys. Rev. Lett.*, 94(10):1–4.

Grolig, F. (1998). Nuclear centering in Spirogyra: force integration by microfilaments along microtubules. *Planta*, 204(1):54–63.

Guesdon, A., Bazile, F., Buey, R. M., Mohan, R., Monier, S., García, R. R., Angevin, M., Heichette, C., Wieneke, R., Tampé, R., Duchesne, L., Akhmanova, A., Steinmetz, M. O., and Chrétien, D. (2016). EB1 interacts with outwardly curved and straight regions of the microtubule lattice. *Nat. Cell Biol.*, 18(10):1102–1108.

Hawkins, R. J., Tindemans, S. H., and Mulder, B. M. (2010). Model for the orientational ordering of the plant microtubule cortical array. *Phys. Rev. E - Stat. Nonlinear, Soft Matter Phys.*, 82(1):011911.

Hertwig, O. (1884). Das Problem der Befruchtung und der Isotropie des Eies, eine Theorie der Vererbung. *Jenaische Zeitschrif fur Naturwissenchaft*, 18:276–318.

Howard, J. (2002). Mechanics of motor proteins and the cytoskeleton. *Phys. Today*, 55(3):63–64.

Hyman, A. A., Salser, S., Drechsel, D. N., Unwin, N., and Mitchison, T. J. (1992). Role of GTP hydrolysis in microtubule dynamics: information from a slowly hydrolyzable analogue, GMPCPP. *Mol. Biol. Cell*, 3(10):1155–67.

Ingber, D. E. (2002). Cancer as a disease of epithelial-mesenchymal interactions and extracellular matrix regulation. *Differentiation*, 70(9-10):547–560.

Jeong, G. J., Oh, J. Y., Kim, Y. J., Bhang, S. H., Jang, H. K., Han, J., Yoon, J. K., Kwon, S. M., Lee, T. I., and Kim, B. S. (2017). Therapeutic Angiogenesis via Solar Cell-Facilitated Electrical Stimulation. *ACS Appl. Mater. Interfaces*, 9(44):38344–38355.

Jürgens, G. (2005). Cytokinesis in higher plants. *Annu. Rev. Plant Biol.*, 56(1):281–299.

Karsenti, E. (2008). Self-organization in cell biology: a brief history. *Nat. Rev. Mol. Cell Biol.*, 9(3):255–62.

Katsuta, J., Hashiguchi, Y., and Shibaoka, H. (1990). The role of the cytoskeleton in positioning of the nucleus in premitotic tobacco BY-2 cells. *J. Cell Sci.*, 95(3):413–422.

Kennard, J. L. and Cleary, A. L. (1997). Pre-mitotic nuclear migration in subsidiary mother cells of Tradescantia occurs in G1 of the cell cycle and requires F-actin. *Cell Motil. Cytoskeleton*, 36(1):55–67.

Kojo, K. H., Higaki, T., Kutsuna, N., Yoshida, Y., Yasuhara, H., and Hasezawa, S. (2013). Roles of cortical actin microfilament patterning in division plane orientation in plants. *Plant Cell Physiol.*, 54(9):1491–1503.

Kunda, P. and Baum, B. (2009). The actin cytoskeleton in spindle assembly and positioning. *Trends Cell Biol.*, 19(4):174–179.

Lang, D., Weiche, B., Timmerhaus, G., Richardt, S., Riano-Pachon, D. M., Correak, L. G., Reski, R., Mueller-Roeber, B., and Rensing, S. A. (2010). Genome-wide phylogenetic comparative analysis of plant transcriptional regulation: A timeline of loss, gain, expansion, and correlation with complexity. *Genome Biol. Evol.*, 2(1):488–503.

Lindeboom, J. J., Lioutas, A., Deinum, E. E., Tindemans, S. H., Ehrhardt, D. W., Mie, A. C., Vos, J. W., and Mulder, B. M. (2013). Cortical microtubule arrays are initiated from a nonrandom prepattern driven by atypical microtubule initiation. *Plant Physiol.*, 161(3):1189–1201.

Liu, B. and Palevitz, B. A. (1992). Organization of cortical microfilaments in dividing root cells. *Cell Motil. Cytoskeleton*, 23(4):252–264.

Lloyd, C. W. and Traas, J. A. (1988). The role of F-actin in determining the division plane of carrot suspension cells . Drug studies. *Development*, 221:211–221.

Louveaux, M., Julien, J. D., Mirabet, V., Boudaoud, A., and Hamant, O. (2016). Cell division plane orientation based on tensile stress in Arabidopsis thaliana. *Proc. Natl. Acad. Sci.*, 113(30):E4294–E4303.

Megraw, T. L. and Kaufman, T. C. (1999). The centrosome in Drosophila oocyte development. *Curr. Top. Dev. Biol.*, 49:385–407.

Minc, N., Burgess, D., and Chang, F. (2011). Influence of cell geometry on division-plane positioning. *Cell*, 144(3):414–426.

Mineyuki, Y. (1999). The preprophase band of microtubules: Its function as a cytokinetic apparatus in higher plants. *Int. Rev. Cytol.*, 187:1–49.

Mineyuki, Y. and Palevitz, B. A. (1990). Relationship between preprophase band organization, F-actin and the division site in Allium. Fluorescence and morphometric studies on cytochalasin-treated cells. *J. Cell Sci.*, 97(2):283–295.

Mirabet, V., Krupinski, P., Hamant, O., Meyerowitz, E. M., Jönsson, H., and Boudaoud, A. (2018). The self-organization of plant microtubules inside the cell volume yields their cortical localization, stable alignment, and sensitivity to external cues. *PLoS Comput. Biol.*, 14(2):e1006011.

Moriwaki, T. and Goshima, G. (2016). Five factors can reconstitute all three phases of microtubule polymerization dynamics. *J. Cell Biol.*, 215(3):357–368.

Morrison, E. E. (2007). Action and interactions at microtubule ends. *Cell. Mol. Life Sci.*, 64(3):307–317.

Müller, S., Wright, A. J., and Smith, L. G. (2009). Division plane control in plants: new players in the band. *Trends Cell Biol.*, 19(4):180–188.

Murata, T. and Wada, M. (1991). Effects of centrifugation on preprophase-band formation in Adiantum protonemata. *Planta*, 183(3):391–398.

Ôta, T. (1961). The Role of Cytoplasm in Cytokinesis of Plant Cells. *Cytology*, 26(3-4):428–447.

Palevitz, B. A. and Hepler, P. K. (1974). The control of the plane of division during stomatal differentiation in Allium - I. Spindle reorientation. *Chromosoma*, 46(3):297–326.

Paluch, E. and Heisenberg, C. P. (2009). Biology and Physics of Cell Shape Changes in Development. *Curr. Biol.*, 19(17):R790–R799.

Panteris, E., Apostolakos, P., and Galatis, B. (1995). The effect of taxol onTriticum preprophase root cells: preprophase microtubule band organization seems to depend on new microtubule assembly. *Protoplasma*, 186(1-2):72–78.

Pease, J. C. and Tirnauer, J. S. (2011). Mitotic spindle misorientation in cancer - out of alignment and into the fire. *J. Cell Sci.*, 124(7):1007–1016.

Pickett-Heaps, J. (1974). The evolution of mitosis and the eukaryotic condition. *BioSystems*, 6(1):37–48.

Pickett-Heaps, J. D. and Northcote, D. H. (1966). Organization of microtubules and endoplasmic reticulum during mitosis and cytokinesis in wheat meristems. *J. Cell Sci.*, 1(1):109–20.

Purswani, N. (2014). *Introducing the gemma of the liverwort Marchantia polymorpha L. as a simple morphogenetic system*. PhD thesis, University of Cambridge.

Ragnarsson, K. T. (2008). Functional electrical stimulation after spinal cord injury: Current use, therapeutic effects and future directions. *Spinal Cord*, 46(4):255–274.

Rappaport, R. (1985). Repeated furrow formation from a single mitotic apparatus in cylindrical sand dollar eggs. *J. Exp. Zool.*, 234(1):167–171.

Rasmussen, C. G., Sun, B., and Smith, L. G. (2011). Tangled localization at the cortical division site of plant cells occurs by several mechanisms. *J. Cell Sci.*, 124(2):270–279.

Rasmussen, C. G., Wright, A. J., and Müller, S. (2013). The role of the cytoskeleton and associated proteins in determination of the plant cell division plane. *Plant J.*, 75(2):258–269.

Reinsch, S. and Gönczy, P. (1998). Mechanisms of nuclear positioning. *J. Cell Sci.*, 111(16):2283–2295.

Sachs, J. (1878). Über die Anordnung der Zellen in jüngsten Pflanzenteilen. *Arb. Bot. Inst. Würzbg.*, 2:46.

Sahlin, P. and Jönsson, H. (2010). A modeling study on how cell division affects properties of epithelial tissues under isotropic growth. *PLoS One*, 5(7):e11750.

Sanderson, M. J., Thorne, J. L., Wikström, N., and Bremer, K. (2004). Molecular evidence on plant divergence times. *Am. J. Bot.*, 91(10):1656–1665.

Schaefer, E., Belcram, K., Uyttewaal, M., Duroc, Y., Goussot, M., Legland, D., Laruelle, E., De Tauzia-Moreau, M. L., Pastuglia, M., and Bouchez, D. (2017). The preprophase band of microtubules controls the robustness of division orientation in plants. *Science*, 356(6334):186–189.

Schmit, A. C. (2002). Acentrosomal microtubule nucleation in higher plants. *Int. Rev. Cytol.*, 220:257–289.

Serna, L. and Fenoll, C. (2003). Stomatal precursors in Arabidopsis: prohibiting the fulfilment of a general rule. *New Phytol.*, 158(3):427–430.

Shapiro, B. E., Tobin, C., Mjolsness, E., and Meyerowitz, E. M. (2015). Analysis of cell division patterns in the Arabidopsis shoot apical meristem. *Proc. Natl. Acad. Sci.*, 112(15):4815–4820.

Smith, L. G. (2001). Plant cell division: building walls in the right places. *Nat Rev Mol Cell Biol*, 2(1):33–39.

Smolarkiewicz, M. and Dhonukshe, P. (2013). Formative cell divisions: Principal determinants of plant morphogenesis. *Plant Cell Physiol.*, 54(3):333–342.

Spinner, L., Gadeyne, A., Belcram, K., Goussot, M., Moison, M., Duroc, Y., Eeckhout, D., De Winne, N., Schaefer, E., Van De Slijke, E., Persiau, G., Witters, E., Gevaert, K., De Jaeger, G., Bouchez, D., Van Damme, D., and Pastuglia, M. (2013). A protein phosphatase 2A complex spatially controls plant cell division. *Nat. Commun.*, 4:1863–1876.

Stoppin-Mellet, V., Gaillard, J., and Vantard, M. (2002). Functional evidence for in vitro microtubule severing by the plant katanin homologue. *Biochem. J.*, 365(2):337–42.

Subramanian, R. and Kapoor, T. M. (2012). Building complexity: insights into self-organized assembly of microtubule-based architectures. *Dev. Cell*, 23(5):874–85.

Sugimoto, K., Williamson, R. E., and Wasteneys, G. O. (2000). New techniques enable comparative analysis of microtubule orientation, wall texture, and growth rate in intact roots of Arabidopsis. *Plant Physiol.*, 124(4):1493–506.

Teixidó-Travesa, N., Roig, J., and Lüders, J. (2012). The where, when and how of microtubule nucleation - one ring to rule them all. *J. Cell Sci.*, 125(19):4445–56.

Thoms, D., Vineyard, L., Elliott, A., and Shaw, S. L. (2018). CLASP facilitates transitions between cortical microtubule array patterns. *Plant Physiol.*, 178(4):1551–1567.

Tindemans, S. H., Hawkins, R. J., and Mulder, B. M. (2010). Survival of the aligned: Ordering of the plant cortical microtubule array. *Phys. Rev. Lett.*, 104(5):1–4.

Van Damme, D. and Geelen, D. (2008). Demarcation of the cortical division zone in dividing plant cells. *Cell Biol. Int.*, 32(2):178–187.

Venverloo, C. J. and Libbenga, K. (1987). Regulation of the Plane of Cell Division in Vacuolated Cells I. The Function of Nuclear Positioning and Phragmosome Formation. *J. Plant Physiol.*, 131(3-4):267–284.

Vineyard, L., Elliott, A., Dhingra, S., Lucas, J. R., and Shaw, S. L. (2013). Progressive transverse microtubule array organization in hormone-induced Arabidopsis hypocotyl cells. *Plant Cell*, 25(2):662–676.

Vos, J. W., Dogterom, M., and Emons, A. M. C. (2004). Microtubules Become More Dynamic but Not Shorter during Preprophase Band Formation: A Possible

"Search-and-Capture" Mechanism for Microtubule Translocation. *Cell Motil. Cytoskeleton*, 57(4):246–258.

Wasteneys, G. O. (2002). Microtubule organization in the green kingdom: Chaos or self-order? *J. Cell Sci.*, 115(7):1345–1354.

Weigert, M., Schmidt, U., Boothe, T., Müller, A., Dibrov, A., Jain, A., Wilhelm, B., Schmidt, D., Broaddus, C., Culley, S., Rocha-Martins, M., Segovia-Miranda, F., Norden, C., Henriques, R., Zerial, M., Solimena, M., Rink, J., Tomancak, P., Royer, L., Jug, F., and Myers, E. W. (2018). Content-aware image restoration: pushing the limits of fluorescence microscopy. *Nat. Methods*, 15(12):1090–1097.

Wu, X., Zhou, J., and Li, D. (2020). Orientation of the mitotic spindle in blood vessel development. *Frontiers in Cell and Developmental Biology*, 8:984.

Wühr, M., Dumont, S., Groen, A. C., Needleman, D. J., and Mitchison, T. J. (2009). How does a millimeter-sized cell find its center? *Cell Cycle*, 8(8):1115–1121.

Yoshida, S., Barbier de Reuille, P., Lane, B., Bassel, G., Prusinkiewicz, P., Smith, R., and Weijers, D. (2014). Genetic Control of Plant Development by Overriding a Geometric Division Rule. *Dev. Cell*, 29(1):75–87.

Zhang, P., Liu, Z. T., He, G. X., Liu, J. P., and Feng, J. (2011). Low-Voltage Direct-Current Stimulation is Safe and Promotes Angiogenesis in Rabbits with Myocardial Infarction. *Cell Biochem. Biophys.*, 59(1):19–27.

Zhao, M., Bai, H., Wang, E., Forrester, J. V., and McCaig, C. D. (2004). Electrical

stimulation directly induces pre-angiogenic responses in vascular endothelial cells by signaling through VEGF receptors. *J. Cell Sci.*, 117(3):397–405.